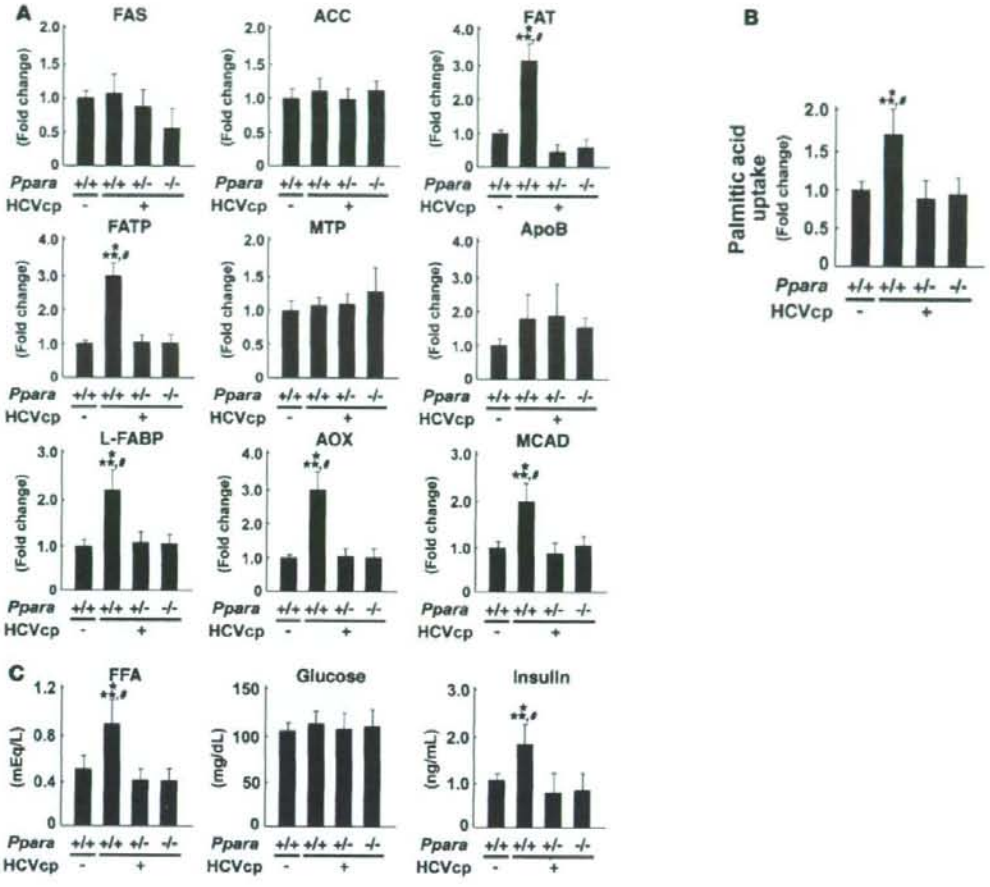

Figure 2

Analyses of factors associated with hepatic fatty acid and triglyceride metabolism. (**A**) Expression of genes associated with fatty acid and triglyceride metabolism in 9-month-old mouse livers. Total RNA was extracted from each mouse liver, and mRNA levels were determined by RT-PCR. mRNA levels were normalized by those of GAPDH and subsequently normalized by those in *Ppara*$^{+/+}$ nontransgenic mice. Results are expressed as the mean ± SD (n = 6/group). *P < 0.05 compared with *Ppara*$^{+/+}$ nontransgenic mice; **P < 0.05 compared with *Ppara*$^{+/-}$:HCVcpTg mice; ♯P < 0.05 compared with *Ppara*$^{-/-}$:HCVcpTg mice. (**B**) Uptake of fatty acids in 9-month-old mouse livers. Liver slices obtained from 3 mice in each group were incubated in medium containing 0.8 mM [1-^{14}C]palmitic acid for 7 h. Fatty acid uptake ability was estimated by the sum of palmitic acid converted to CO_2 and ketone bodies with that incorporated into total cellular lipids after incubation. The experiment was repeated 3 times. Results were normalized by those of *Ppara*$^{+/+}$ nontransgenic mice and expressed as the mean ± SD. (**C**) Plasma concentrations of free fatty acids, glucose, and insulin. After an overnight fast, blood was obtained from each mouse and the above variables were determined. Results are expressed as the mean ± SD (n = 6/group).

degeneration and necrosis, and fibrosis were not detected. On the other hand, *Ppara*$^{+/-}$:HCVcpTg and *Ppara*$^{-/-}$:HCVcpTg mice showed no steatosis (Figure 1, C and D). These results indicate that hepatic steatosis develops in *Ppara*$^{+/+}$:HCVcpTg mice, but not in *Ppara*$^{+/-}$:HCVcpTg and *Ppara*$^{-/-}$:HCVcpTg mice.

Hepatic fatty acid and triglyceride metabolism in transgenic mice. To investigate the mechanism responsible for the development of severe steatosis in *Ppara*$^{+/+}$:HCVcpTg mice, the expression of genes associated with fatty acid and triglyceride metabolism in the livers of 9-month-old mice was analyzed using the quantitative RT-PCR method. As shown in Figure 2A, the mRNA levels of genes related to de novo lipogenesis (fatty acid synthase [FAS] and acetyl-CoA carboxylase [ACC]) and secretion of VLDL (microsomal transfer protein [MTP] and apoB) were constant in all groups. The mRNA levels of fatty acid translocase (FAT) and fatty acid transport protein (FATP), which are associated with the uptake of fatty acids into hepatocytes, were significantly increased only in *Ppara*$^{+/+}$:HCVcpTg mice, but the mRNA levels of hepatic triglyceride lipase, another contributor to fatty acid uptake, remained unchanged (data not shown). The mRNA levels of liver fatty acid binding protein (L-FABP) were also elevated only in *Ppara*$^{+/+}$:HCVcpTg mice. Surprisingly, the mRNA levels of AOX and medium-chain acyl-CoA

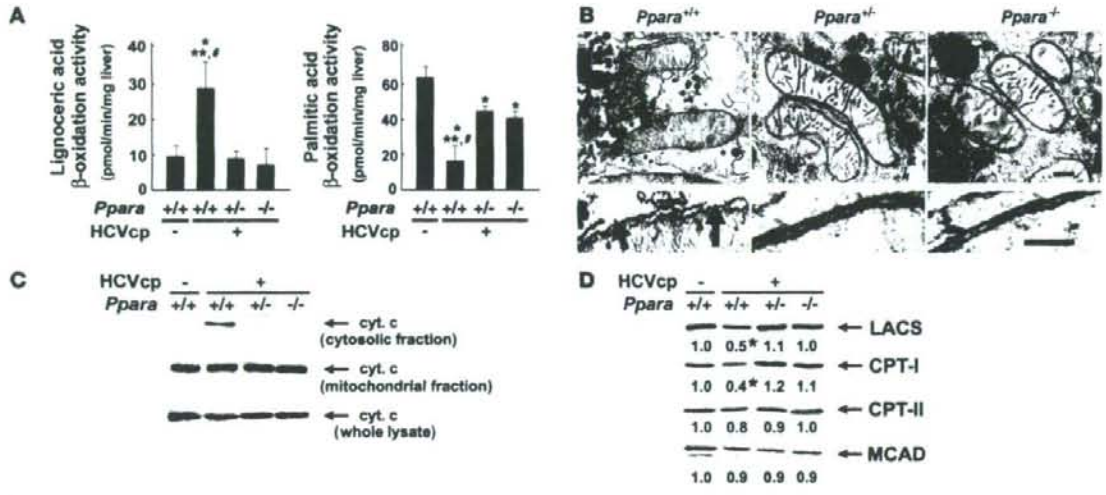

Figure 3

Analyses of mitochondrial abnormalities. (**A**) Lignoceric and palmitic acid β-oxidation activities in 9-month-old mice. Results are expressed as the mean ± SD (n = 6/group). *P < 0.05 compared with *Ppara*$^{+/+}$ nontransgenic mice; **P < 0.05 compared with *Ppara*$^{+/-}$:HCVcpTg mice; #P < 0.05 compared with *Ppara*$^{-/-}$:HCVcpTg mice. (**B**) Electron microscopic features of hepatic mitochondria of 9-month-old HCVcpTg mice. Upper and lower rows show a lower and higher magnification, respectively. In *Ppara*$^{+/+}$:HCVcpTg mice, some mitochondria showing discontinuance of outer membranes (arrows) and amorphous inner structures were observed. In *Ppara*$^{+/-}$:HCVcpTg and *Ppara*$^{-/-}$:HCVcpTg mice, mitochondria appeared normal; the scale bars represent 200 nm (top) and 30 nm (bottom), respectively. (**C**) Immunoblot analysis of cytochrome *c* in 9-month-old mice. Whole-liver lysate, mitochondrial fraction, or cytosolic fraction (50 μg protein) was loaded in each well. Results are representative of 4 independent experiments. (**D**) Immunoblot analysis of representative mitochondrial β-oxidation enzymes using a mitochondrial fraction prepared from 9-month-old mouse livers. The mitochondrial fraction (20 μg protein) was loaded in each well. Results are representative of 4 independent experiments. The band intensity was quantified densitometrically and normalized by that in *Ppara*$^{+/+}$ nontransgenic mouse. The mean value of the fold changes is shown under the representative band. LACS, long-chain acyl-CoA synthase; CPT, carnitine palmitoyl-CoA transferase.

dehydrogenase (MCAD), a rate-limiting enzymes in the peroxisomal and mitochondrial β-oxidation pathways, respectively, were significantly increased in *Ppara*$^{+/+}$:HCVcpTg mice. When fatty acid uptake ability was measured in fresh liver slices, it was significantly enhanced only in *Ppara*$^{+/+}$:HCVcpTg mice (Figure 2B). Additionally, plasma free fatty acid levels were higher in these mice than in mice in the other groups. Although there were no differences in fasting plasma glucose levels between the groups, hyperinsulinemia was observed only in *Ppara*$^{+/+}$:HCVcpTg mice (Figure 2C), in agreement with the previous observation that significant insulin resistance developed in these mice (8). Similar results were obtained from 24-month-old mice (data not shown). These results combined show that the increased plasma fatty acid levels, which were likely due to enhanced peripheral fatty acid release caused by insulin resistance, and the increase in fatty acid uptake ability are consistent with steatogenesis in *Ppara*$^{+/+}$:HCVcpTg mice.

Decreased mitochondrial β-oxidation in transgenic mice. Although the transcriptional activities of major β-oxidation enzymes were markedly increased, *Ppara*$^{+/+}$:HCVcpTg mice had severe steatosis. To explore this discrepant result, peroxisomal and mitochondrial β-oxidation activities were measured using lignoceric and palmitic acids as substrates, respectively. The lignoceric acid–degrading capacity was increased only in *Ppara*$^{+/+}$:HCVcpTg mice, where it corresponded to an increase in AOX expression. However, the capacity for palmitic acid degradation, which occurs particularly in mitochondria, was significantly lower in *Ppara*$^{+/+}$:HCVcpTg mice than in *Ppara*$^{+/-}$:HCVcpTg and *Ppara*$^{-/-}$:HCVcpTg mice (Figure 3A). Thus, decreased mitochondrial β-oxidation ability was considered to be another important mechanism for the development of steatosis induced by the core protein.

We further evaluated mitochondrial abnormalities. In electron microscopic examination, discontinuous outer membranes (Figure 3B, arrows) and lack of an internal structure were observed in some mitochondria of *Ppara*$^{+/+}$:HCVcpTg mouse livers, in agreement with the previous report (9). However, these abnormalities were not seen in *Ppara*$^{+/-}$:HCVcpTg and *Ppara*$^{-/-}$:HCVcpTg mice (Figure 3B). Immunoblot analysis showed that cytochrome *c*, which is usually localized in the mitochondrial intermembrane space, was present in the cytosolic fractions of *Ppara*$^{+/+}$:HCVcpTg mice (Figure 3C). Moreover, immunoblot analysis using mitochondrial fractions showed that the expression levels of long-chain acyl-CoA synthase and carnitine palmitoyl-CoA transferase-I, which are enzymes indispensable to the initial step of mitochondrial β-oxidation and are localized mainly in mitochondrial outer membranes, were significantly decreased only in *Ppara*$^{+/+}$:HCVcpTg mice (Figure 3D).

Overall, these results suggest that homozygous PPARα is essential to the pathogenesis of hepatic steatosis induced by the HCV core protein, which results from a decrease in mitochondrial fatty acid degradation capacity caused by the breakdown of mitochondrial outer membranes and a disproportionate increase in the uptake of fatty acids. Interestingly, steatosis and the related changes did not occur in *Ppara*$^{+/-}$ and *Ppara*$^{-/-}$ mice expressing the HCV core protein, which suggested that these changes were not caused by the core protein itself.

Table 1
Incidence of HCC in 24-month-old mice

HCV core protein	*Ppara*	Mice (*n*)	Mice with HCC (*n*)	Incidence (%)
–	+/+	20	0	0
–	+/–	18	0	0
–	–/–	20	0	0
+	+/+	17	6	35.3[A]
+	+/–	16	0	0
+	–/–	14	0	0

Mice were killed at 24 months of age for analysis. HCC was diagnosed according to histological findings. [A]$P < 0.05$ compared with *Ppara*$^{+/+}$ nontransgenic mice, $P < 0.05$ compared with *Ppara*$^{+/-}$:HCVcpTg mice, $P < 0.05$ compared with *Ppara*$^{-/-}$:HCVcpTg mice.

Requirement of homozygous PPARα for hepatic tumor development in transgenic mice. At 9 months of age, hepatic nodules were not observed at all in transgenic mice, whereas, at 24 months, approximately 35% of *Ppara*$^{+/+}$:HCVcpTg mice had macroscopically evident hepatic nodules (Table 1). Microscopically, these nodules had the appearance of well-differentiated HCC with trabecular features, which was consistent with the previous report (9). Surprisingly, *Ppara*$^{+/-}$:HCVcpTg and *Ppara*$^{-/-}$:HCVcpTg mice of the same ages developed no evidence of hepatic tumors, despite the expression of HCV core protein at similar levels to those found in *Ppara*$^{+/+}$:HCVcpTg mice (Table 1). Microscopic examination showed that there were no dysplastic cells or precancerous lesions throughout the livers in *Ppara*$^{+/-}$:HCVcpTg and *Ppara*$^{-/-}$:HCVcpTg mice (Figure 1C). These results provide strong evidence that homozygous PPARα is essential for hepatic tumorigenesis induced by HCV core protein.

Increased hepatocyte proliferation only in Ppara$^{+/+}$*:HCVcpTg mice.* Because sustained acceleration of hepatocyte proliferation relative to apoptosis may promote the development of HCC, these opposing processes were quantified in the livers of 24-month-old mice. Both the liver-to-body weight ratio and the number of hepatocytes expressing proliferating cell nuclear antigen (PCNA) were increased only in *Ppara*$^{+/+}$:HCVcpTg mice (Figure 4, A and B). In contrast, the number of TUNEL-positive hepatocytes and the hepatic caspase 3 activity, indicators of hepatocyte apoptosis, remained similar among the 3 mouse strains (Figure 4, C and D). Interestingly, despite the presence of HCV core protein, the amounts of these proliferative and apoptotic markers in *Ppara*$^{+/-}$:HCVcpTg and *Ppara*$^{-/-}$:HCVcpTg mice were similar to those in *Ppara*$^{+/+}$ nontransgenic mice. Expression levels of several proteins, such as protooncogenes (c-Fos and c-Myc), cell-cycle regulators (cyclin D1, cyclin-dependent kinase [CDK] 4, and PCNA), and phosphorylated ERK 1 and 2, all of which are associated with hepatocyte proliferation, were elevated in *Ppara*$^{+/+}$:HCVcpTg mice but not in other genotypes (Figure 4, E and F).

Increased oxidative stress and DNA damage only in Ppara$^{+/+}$*:HCVcpTg mice.* HCV core protein is associated with increased production of ROS (23). Enhanced ROS production induces nuclear DNA damage, which results in the initiation of hepatocarcinogenesis, and can also injure organelles, which can result in disorders in their

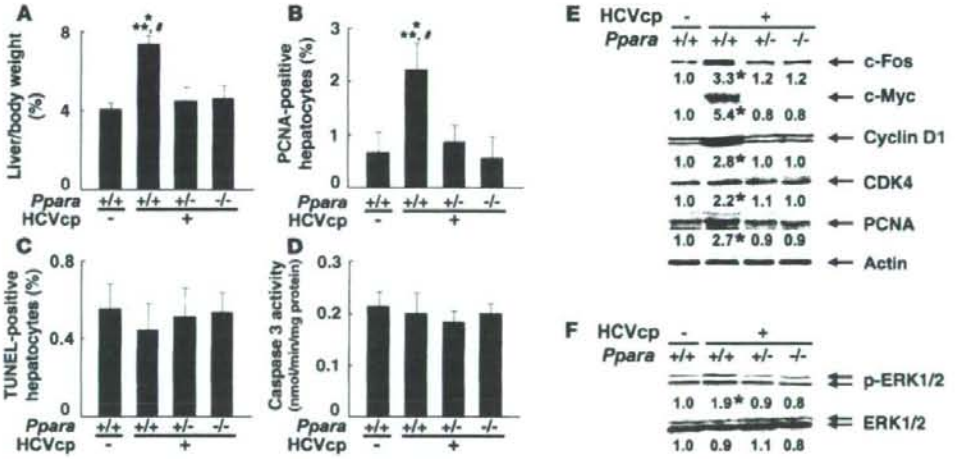

Figure 4
Increased hepatocyte proliferation in *Ppara*$^{+/+}$:HCVcpTg mice at 24 months of age. (**A**) Liver-to-body-weight ratio. Results are expressed as the mean ± SD (n = 6/group). (**B**) Numbers of proliferating hepatocytes. Two thousand hepatocytes were examined in each mouse, and hepatocyte nuclei positive for anti-PCNA antibody were counted. Results are expressed as the mean ± SD (n = 6/group). For **A** and **B**, comparisons are designated as follows: *$P < 0.05$ compared with *Ppara*$^{+/+}$ nontransgenic mice; **$P < 0.05$ compared with *Ppara*$^{+/-}$:HCVcpTg mice; #$P < 0.05$ compared with *Ppara*$^{-/-}$:HCVcpTg mice. (**C**) Numbers of apoptotic hepatocytes. Liver sections were subjected to TUNEL staining, and TUNEL-positive hepatocyte nuclei were counted in 2,000 hepatocytes from each mouse. Results are expressed as the mean ± SD (n = 6/group). (**D**) Caspase 3 activity. Results are expressed as the mean ± SD (n = 6/group). (**E**) Immunoblot analysis of oncogene products and cell cycle regulators. The same sample used in Figure 1A (whole-liver lysate, 50 μg protein) was loaded in each well. The band of actin was used as the loading control. Results are representative of 4 independent experiments. The band intensity was quantified densitometrically, normalized by that of actin, and subsequently normalized by that in *Ppara*$^{+/+}$ nontransgenic mice. The mean value of the fold changes is expressed under each band. (**F**) Immunoblot analysis of phosphorylated ERK1/2 and total ERK1/2. The same samples in Figure 4E (50 μg protein) were used.

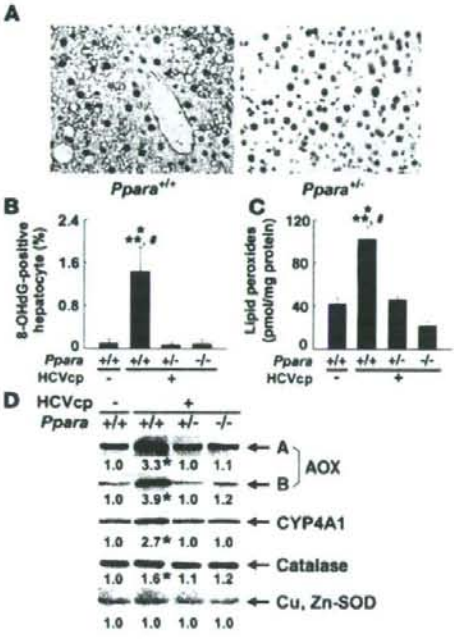

Figure 5
Increased oxidative stress and DNA damage in *Ppara*$^{+/+}$:HCVcpTg mice at 24 months of age. (**A**) Immunohistochemical staining using antibody against 8-OHdG. In *Ppara*$^{+/+}$:HCVcpTg mice, some steatotic hepatocytes were positive for 8-OHdG. Original magnification, ×400. (**B**) Numbers of 8-OHdG–positive hepatocytes. Hepatocyte nuclei stained with anti-8-OHdG antibody were counted in 2,000 hepatocytes of each mouse. Results are expressed as the mean ± SD (n = 6/group). (**C**) Hepatic content of lipid peroxides. Results are expressed as the mean ± SD (n = 6 /group). $^{*}P < 0.05$ compared with *Ppara*$^{+/+}$ nontransgenic mice; $^{**}P < 0.05$ compared with *Ppara*$^{+/-}$:HCVcpTg mice; $^{\#}P < 0.05$ compared with *Ppara*$^{-/-}$:HCVcpTg mice. (**D**) Immunoblot analysis of AOX, CYP4A1, catalase, and Cu, Zn-SOD. The whole-liver lysate used in the experiment in Figure 4E (20 μg protein for AOX and CYP4A1 and 50 μg for others) was loaded in each lane. The band of actin was used as the loading control. Results are representative of 4 independent experiments. **A** and **B** indicate full-length and truncated AOX, respectively. The band intensity was quantified densitometrically, normalized by that of actin, and subsequently normalized by that in *Ppara*$^{+/+}$ nontransgenic mice. The mean value of the fold changes is expressed under each band. $^{*}P < 0.05$ compared with *Ppara*$^{+/+}$ nontransgenic mice.

function. The number of hepatocytes positive for 8-hydroxy-2′-deoxyguanosine (8-OHdG), an indicator of oxidative damage to nuclear DNA, was increased only in 24-month-old *Ppara*$^{+/+}$:HCVcpTg mice (Figure 5, A and B). Lipid peroxides were slightly increased in the livers of 9-month-old *Ppara*$^{+/+}$:HCVcpTg mice (data not shown) and were more abundant in the livers of 24-month-old *Ppara*$^{+/+}$:HCVcpTg mice than in those of *Ppara*$^{+/-}$:HCVcpTg and *Ppara*$^{-/-}$:HCVcpTg mice or *Ppara*$^{+/+}$ nontransgenic mice (Figure 5C). Expression of typical ROS-generating enzymes (AOX and cytochrome P450 4A1 [CYP4A1]) and ROS-eliminating enzymes (catalase and Cu, Zn-SOD) was examined. Immunoblot analysis showed marked increases in the expression of AOX and CYP4A1 and mild increases in that of catalase only in *Ppara*$^{+/+}$:HCVcpTg mice. No changes in Cu, Zn-SOD were found in the subgroups of transgenic mice (Figure 5D). These results suggest that enhanced oxidative stress causes damage in nuclear DNA and probably in mitochondria in the *Ppara*$^{+/+}$:HCVcpTg mice.

Persistent and spontaneous PPARα activation in Ppara$^{+/+}$*:HCVcpTg mice.* Liver tumorigenesis induced by long-term exposure to peroxisome proliferators and the related changes, such as sustained hepatocyte proliferation and increased oxidative stress, are associated with persistent PPARα activation (19–21). To examine the activation of PPARα, we quantified the level of PPARα mRNA, which is induced by PPARα activation (24, 25). PPARα mRNA levels were higher in 9-month-old *Ppara*$^{+/+}$:HCVcpTg mice than in *Ppara*$^{+/+}$ nontransgenic mice (Figure 6A). These increases were more pronounced at 24 months of age. However, there were no differences in PPARα mRNA levels between *Ppara*$^{+/-}$:HCVcpTg and *Ppara*$^{+/-}$ nontransgenic mice at either 9 or 24 months of age. The expression levels of typical PPARα target genes (16, 25, 26) — such as FAT, FATP, L-FABP, AOX, and MCAD (Figure 2); c-Myc, cyclin D1, CDK4, and PCNA (Figure 4); and CYP4A1 (Figure 5) — were simultaneously and synchronously increased in *Ppara*$^{+/+}$:HCVcpTg mice, but not in *Ppara*$^{+/-}$:HCVcpTg or *Ppara*$^{-/-}$:HCVcpTg mice. These results confirm that persistent activation of PPARα occurs only in *Ppara*$^{+/+}$:HCVcpTg mice. Various changes observed in *Ppara*$^{+/+}$:HCVcpTg mice, i.e., increased fatty acid uptake, mitochondrial abnormalities, steatosis, ROS overproduction, accelerated hepatocyte proliferation, and hepatocarcinogenesis, were considered to be closely linked with sustained PPARα activation.

Nuclear PPARα content. The results described above suggest that persistent PPARα activation is critical to the steatogenesis and hepatocarcinogenesis induced by the HCV core protein. A question arises as to why *Ppara*$^{+/-}$:HCVcpTg mice with an active *Ppara* allele do not exhibit the hallmarks of PPARα activation and do not develop HCC. To address this issue, the nuclear PPARα content was analyzed. Immunoblot analysis for PPARα showed that the amount of nuclear PPARα protein in *Ppara*$^{+/+}$:HCVcpTg mice was approximately 2- to 3-fold that of *Ppara*$^{+/+}$ nontransgenic mice, which was disproportionate to the higher PPARα mRNA levels (approximately 1.2- to 1.6-fold) (Figure 6, A and B). The level of nuclear PPARα in *Ppara*$^{+/-}$:HCVcpTg mice was significantly lower than that in *Ppara*$^{+/+}$:HCVcpTg mice and was similar to that in *Ppara*$^{+/+}$ nontransgenic mice (Figure 6B). Thus, the lower amount of nuclear PPARα in *Ppara*$^{+/-}$:HCVcpTg mice than in *Ppara*$^{+/+}$:HCVcpTg mice might have heightened the threshold of expression required for long-term spontaneous PPARα activation.

The degree of an increase in nuclear PPARα levels was evidently higher than the degree of an increase in PPARα mRNA levels in HCVcpTg mice (Figure 6, A and B). To investigate this disparity, the stability of nuclear PPARα was evaluated by pulse-chase experiments using isolated hepatocytes obtained from these mice. The half-life of nuclear PPARα was significantly longer ($P < 0.05$) in *Ppara*$^{+/+}$:HCVcpTg mice (11.5 ± 2.3 h) than in *Ppara*$^{+/+}$ nontransgenic mice (5.8 ± 1.4 h) (Figure 6C). The half-life of nuclear PPARα in *Ppara*$^{+/-}$:HCVcpTg mice tended to be prolonged compared with that in *Ppara*$^{+/-}$ nontransgenic mice (Figure 6C). These results suggest that the stability of nuclear PPARα was increased as a result of HCV core protein expression. Because it is known that the core protein interacts with retinoid X receptor α (RXRα) (27) and that

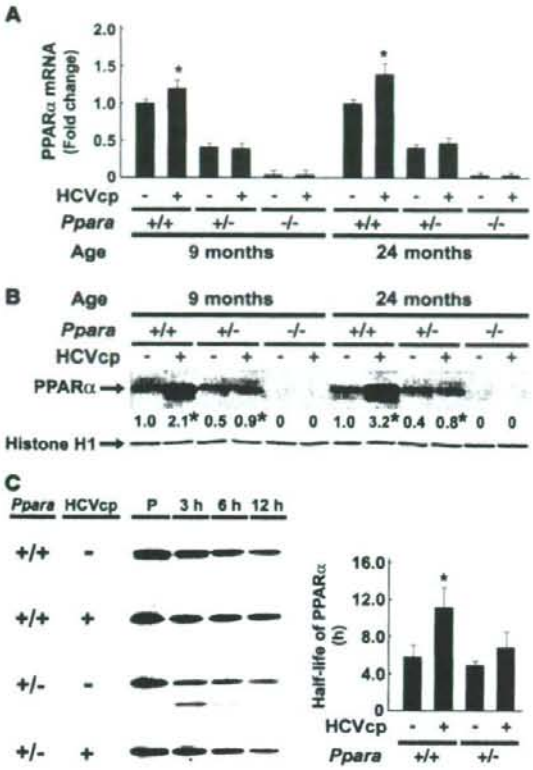

Figure 6

Persistent PPARα activation in *Ppara*$^{+/+}$:HCVcpTg mice. (**A**) PPARα mRNA levels. Total RNA was prepared from each mouse, and PPARα mRNA levels were determined by RT-PCR, normalized by those of GAPDH, and subsequently normalized by those of 9-month-old *Ppara*$^{+/+}$ nontransgenic mice. Results are expressed as the mean ± SD (n = 6 /group). (**B**) Immunoblot analysis of nuclear PPARα. The nuclear fraction obtained from each mouse (100 μg protein) was loaded in each well. The band of histone H1 was used as the loading control. Results are representative of 6 independent experiments. The band intensity was quantified densitometrically, normalized by that of histone H1, and subsequently normalized by that in 9-month-old *Ppara*$^{+/+}$ nontransgenic mice. The mean value is expressed under each band. *P < 0.05 compared with nontransgenic mice of the same age and *Ppara* genotype. (**C**) Pulse-chase experiments for 3, 6, and 12 h and pulse-label (P) experiments for nuclear PPARα using isolated mouse hepatocytes. Left: labeled PPARα bands on x-ray film. Pulse-label and pulse-chase experiments were performed as described in Methods. Results are representative of 4 independent experiments. Right: half-life of PPARα. The band intensity was measured densitometrically and subsequently normalized by that of the pulse-label experiments. The percentage of the band intensity was plotted, and the half-life of PPARα was calculated. Results obtained from 4 independent experiments are expressed as the mean ± SD. *P < 0.05 compared with nontransgenic mice in the same *Ppara* genotype.

PPARα influences the stability of RXRα (28), it is plausible that the core protein would affect its action in nuclei through an interaction with the PPARα-RXRα heterodimer and stabilization of PPARα.

Development of hepatic steatosis and HCC with long-term clofibrate treatment in Ppara$^{+/-}$*:HCVcpTg mice.* To further confirm the significance of persistent PPARα activation on core protein–induced pathological changes, *Ppara*$^{+/-}$ and *Ppara*$^{+/-}$:HCVcpTg mice were fed a standard diet containing 0.05% clofibrate for 24 months. Interestingly, hepatic steatosis appeared in the clofibrate-treated *Ppara*$^{+/-}$:HCVcpTg mice, but not in the *Ppara*$^{+/-}$ mice under the same treatment conditions (Figure 7, A and B). Similar to our observations in *Ppara*$^{+/+}$:HCVcpTg mice not treated with clofibrate, aberrant mitochondria with discontinuous outer membranes and decreased palmitic acid β-oxidation activity were found only in the clofibrate-treated *Ppara*$^{+/-}$:HCVcpTg mice (Figure 7, A and C). In addition, levels of MCAD mRNA; AOX, and CYP4A1 proteins; PPARα mRNA; and nuclear PPARα protein were higher in the clofibrate-treated *Ppara*$^{+/-}$:HCVcpTg mice than in the clofibrate-treated *Ppara*$^{+/-}$ mice (Figure 7, D–F), which suggests that the degree of PPARα activation in the former group was greater than that in the latter group and similar to that in *Ppara*$^{+/+}$:HCVcpTg mice not treated with clofibrate. Finally, the incidence of HCC after clofibrate treatment was higher in *Ppara*$^{+/-}$:HCVcpTg mice (25%; 5 in 20 mice) than in *Ppara*$^{+/-}$ mice (5%; 1 in 20 mice). Therefore, these results corroborate the importance of constant PPARα activation to the pathogenesis of hepatic steatosis and HCC in the transgenic mice.

Discussion

A novel and striking finding in this study is the absolute requirement of persistent PPARα activation for the development of HCV core protein–induced steatosis and HCC. Our data also show that the HCV core protein alone cannot induce steatosis and HCC in transgenic mice.

Mechanisms of development of steatosis in HCVcpTg mice were previously explained as an enhancement of de novo synthesis of fatty acids (29) and a decrease in MTP expression, the latter of which results in insufficient VLDL secretion from hepatocytes (30). In the present study, we revealed 2 novel mechanisms of steatogenesis in the transgenic mice, i.e., an impairment of mitochondrial β-oxidation due to the breakdown of mitochondrial outer membranes and an increase in fatty acid uptake into hepatocytes, associated with PPARα activation. PPARα activation, mitochondrial dysfunction, and hepatic steatosis appeared in 9-month-old *Ppara*$^{+/+}$:HCVcpTg mice and continued until 24 months of age, clearly preceding development of HCC. These findings thereby indicate a correlation between PPARα activation, hepatic steatosis, and HCC.

We obtained the novel and rather paradoxical finding that significant PPARα activation, which generally is expected to reduce hepatic triglyceride levels, is essential for the development of severe steatosis induced by HCV core protein. According to the results of this study, the following hypothesis concerning the development of steatosis in *Ppara*$^{+/+}$:HCVcpTg mice is proposed. First, the HCV core protein localizes partly in mitochondria (9). A recent study

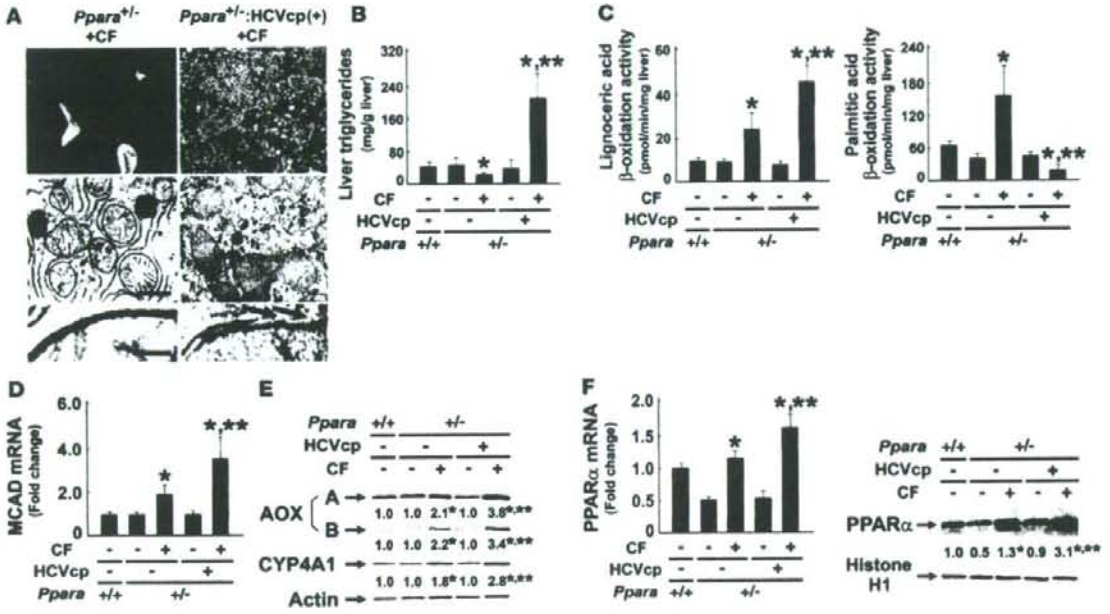

Figure 7

Development of hepatic steatosis by long-term treatment of clofibrate in *Ppara*$^{+/-}$:HCVcpTg mice. (**A**) Histological examination of *Ppara*$^{+/-}$ and *Ppara*$^{+/-}$:HCVcpTg mice treated with diet containing 0.05% (w/w) clofibrate for 24 months (CF). Top: Histological appearance of H&E-stained liver sections. Magnification, ×40. Microvesicular and macrovesicular steatosis were detected only in clofibrate-treated *Ppara*$^{+/-}$:HCVcpTg mice. Middle and bottom: Electron microscopic features of hepatic mitochondria. Some *C*-shaped mitochondria showing discontinuance of outer membranes (arrows) were found in clofibrate-treated *Ppara*$^{+/-}$:HCVcpTg mice. Scale bars: 400 nm (middle), 30 nm (bottom). (**B** and **C**) Content of liver triglycerides and lignoceric and palmitic acid β-oxidation activities. (**D**) MCAD mRNA levels. mRNA levels were normalized to those of GAPDH and subsequently normalized to those in *Ppara*$^{+/+}$ nontransgenic mice. (**E**) Immunoblot analysis of AOX and CYP4A1. Whole-liver lysate (20 μg protein) was loaded in each lane. Actin was used as a loading control. Results are representative of 6 independent experiments. (**F**) PPARα mRNA levels and nuclear PPARα contents. Left: PPARα mRNA levels. The same samples used in **D** were adopted. Right: Immunoblot analysis of nuclear PPARα. Nuclear fraction obtained from each mouse (100 μg protein) was loaded in each well. Histone H1 was used as a loading control. In **E** and **F**, the mean value of the fold changes is shown under each band. Results are representative of 6 independent experiments. Band intensity was quantified densitometrically, normalized to that of the loading control, and subsequently normalized to that in *Ppara*$^{+/+}$ nontransgenic mice. $^{*}P < 0.05$ compared with untreated mice of the same genotype; $^{**}P < 0.05$ compared with clofibrate-treated *Ppara*$^{+/-}$ mice without core protein gene. Results are expressed as mean ± SD (n = 6/group).

showed that, in isolated mitochondria, the core protein directly increased Ca^{2+} influx, inhibited electron transport complex I activity, and induced ROS production (31), all of which can increase the fragility of mitochondria and depress mitochondrial function. In addition, the HCV core protein also localizes in nuclei (9) and can coexist in PPARα-RXRα heterodimer through a direct interaction with the DNA-binding domain of RXRα, which enhances the transcriptional activity of PPARα target genes, such as AOX, despite the absence of PPARα ligands in cultured cells (27). The HCV core protein can also be involved in the PPARα-RXRα complex through a direct interaction with cyclic-AMP responsive element binding protein-binding protein (32), which is able to bind to PPARα (33). Thus, the core protein probably serves as a coactivator and stabilizer of PPARα in vivo, which was further confirmed in this study. Moreover, because it is also known that the core protein itself activates ERK1/2 and p38 mitogen-activated protein kinase (34), these activations might phosphorylate PPARα and thereby transactivate it (35). The core protein–induced PPARα activation enhances the basal expression of AOX and CYP4A1, which leads to increased production of ROS and dicarboxylic acids. These toxic compounds can damage mitochondrial outer membranes, which impairs the mitochondrial β-oxidation system. These damages directly induce the accumulation of long-chain fatty acids in hepatocytes. Furthermore, PPARα activation increases the expression of FAT and FATP, which promotes the influx of fatty acids from blood. Long-chain fatty acids and their CoA esters accumulated in hepatocytes are likely to act as potent detergents, which further damages the outer membranes of mitochondria. Fatty acids and their derivatives function as natural ligands of PPARα, which results in the activation of PPARα and the induction of FAT, FATP, AOX, and CYP4A1, which further accelerates mitochondrial damage, the reduction of mitochondrial β-oxidation activity, and the accumulation of fatty acids in a vicious cycle.

Persistent PPARα activation increases oxidative DNA damage because of a disproportionate increase in ROS-generating enzymes relative to the levels of degrading enzymes such as catalase and SOD, which can predispose hepatocytes to malignant transformation. In addition, persistent PPARα activation leads to increased

Table 2
Primer pairs used for RT-PCR

Gene	GeneBank accession number		Primer sequence	Product (bp)
ACC	NM_133360	F	5′-GGGCACAGACCGTGGTAGTT-3′	105
		R	5′-CAGGATCAGCTGGGATACTGAGT-3′	
ApoB	NM_009693	F	5′-TCACCCCCGGGATCAAG-3′	85
		R	5′-TCCAAGGACACAGAGGGCTTT-3′	
AOX	NM_015729	F	5′-TGGTATGGTGTCGTACTTGAATGAC-3′	145
		R	5′-AATTTCTACCAATCTGGCTGCAC-3′	
FAS	NM_007988	F	5′-ATCCTGGAACGAGAACACGATCT-3′	140
		R	5′-AGAGACGTGTCACTCCTGGACTT-3′	
FAT	NM_007643	F	5′-CCAAATGAAGATGAGCATAGGACAT-3′	87
		R	5′-GTTGACCTGCAGTCGTTTTGC-3′	
FATP	NM_011977	F	5′-ACCACCGGGCTTCCTAAGG-3′	80
		R	5′-CTGTAGGAATGGTGGCCAAAG-3′	
GAPDH	M32599	F	5′-TGCACCACCAACTGCTTAG-3′	177
		R	5′-GGATGCAGGGATGATGTTCTG-3′	
L-FABP	NM_017399	F	5′-GCAGAGCCAGGAGAACTTTGAG-3′	121
		R	5′-TTTGATTTTCTTCCCTTCATGCA-3′	
MCAD	NM_007382	F	5′-TGCTTTTGATAGAACCAGACCTACAGT-3′	128
		R	5′-CTTGGTGCTCCACTAGCAGCTT-3′	
MTP	NM_008642	F	5′-GAGCGGTCTGGATTTACAACG-3′	72
		R	5′-GTAGGTAGTGACAGATGTGGCTTTTG-3′	
PPARα	NM_011144	F	5′-CCTCAGGGTACCACTACGGAGT-3′	69
		R	5′-GCCGAATAGTTCGCCGAA-3′	

F, forward sequence; R, reverse sequence.

cell division, as revealed by the expression of cell cycle regulators such as cyclin D1 and CDK4. Furthermore, there is little change in apoptosis, which, under normal circumstances, would remove damaged cells capable of undergoing transformation. Thus, under these conditions, it is plausible that some aberrant hepatocytes do not undergo apoptosis and develop into HCC.

It is well known that chronic activation of PPARα is associated with hepatocarcinogenesis in mice exposed to peroxisome proliferators or in mice lacking AOX expression. The common clinicopathological characteristics of HCC in these mice are multicentric HCC (20, 22, 36, 37), the well-differentiated appearance of HCC including trabecular features and often a "nodule-in-nodule" pattern (22, 36, 37), and no evidence of fibrosis or cirrhosis in the nonneoplastic liver parenchyma (22, 36), similar to that observed in *Ppara*$^{+/+}$:HCVcpTg mice. However, mice chronically exposed to peroxisome proliferators are clearly distinct from *Ppara*$^{+/+}$:HCVcpTg mice in that they have normal mitochondrial organization, increased mitochondrial β-oxidation activity, and no steatosis (16, 36). AOX-null mice are also different from *Ppara*$^{+/+}$:HCVcpTg mice with respect to mitochondrial structure (22). These detailed comparisons between the 3 mouse models reveal the importance of mitochondrial abnormalities in the pathogenesis of HCV-related diseases.

PPARα is known to regulate the hepatic expression of many proteins associated with fatty acid and triglyceride metabolism, cell division and apoptosis, oxidative stress generation and degradation, and so forth (15, 16, 20, 21, 24–26); therefore, complete deletion of the PPARα gene from mice might cause hitherto unknown influences on the pathways involved in the development of hepatic steatosis and HCC. To consider these unknown effects, *Ppara*$^{+/-}$:HCVcpTg mice were adopted in the current study. Surprisingly, almost all results from *Ppara*$^{+/-}$:HCVcpTg mice were similar to those from *Ppara*$^{-/-}$:HCVcpTg mice, which demonstrates that the presence of functional PPARα itself is not a prerequisite for the occurrence of steatosis and HCC induced by the HCV core protein. Moreover, a comparison between *Ppara*$^{+/-}$:HCVcpTg and *Ppara*$^{+/+}$:HCVcpTg mice uncovered an unexpected and important fact that the core protein–dependent pathological changes do not appear without significant activation of PPARα. Thus, it is not the presence of PPARα per se, but rather a high level of PPARα activation that seems to be essential for the development of HCV core protein–induced steatosis and HCC.

To reinforce the abovementioned hypothesis, *Ppara*$^{+/-}$ and *Ppara*$^{+/-}$:HCVcpTg mice were treated with an exogenous PPAR agonist, clofibrate, for 24 months. In *Ppara*$^{+/-}$ mice, long-term clofibrate treatment caused a certain level of persistent PPARα activation and a low incidence of HCC. Interestingly, in *Ppara*$^{+/-}$:HCVcpTg mice, clofibrate treatment induced more intensive PPARα activation and HCC at a much higher incidence, accompanied by damaged mitochondrial outer membranes, severe steatosis, and decreased mitochondrial β-oxidation activity. The results from the clofibrate-treated *Ppara*$^{+/-}$:HCVcpTg mice were similar to those of the *Ppara*$^{+/+}$:HCVcpTg mice not treated with clofibrate. Therefore, these findings further support the concept that a long-term and high level of PPARα activation is necessary for steatogenesis and hepatocarcinogenesis in HCVcpTg mice and emphasize the significant role of the HCV core protein as a PPARα coactivator in vivo.

A pulse-chase experiment showed that PPARα was stabilized in hepatocyte nuclei in mice expressing the HCV core protein. Many nuclear receptors, including PPARα and RXRα, are known to be degraded by the ubiquitin-proteasome system (38), which plays an important role in modulating the activity of nuclear receptors. Further studies will be needed to clarify whether the core protein influences the ubiquitin-proteasome pathway.

Recent studies have shown conflicting result, i.e., that PPARα was downregulated in the livers of chronic hepatitis C patients (39, 40). Although the association between PPARα function and chronic HCV infection remains a matter of controversy in humans, the changes observed in the transgenic mice resemble in many ways the clinicopathological features of chronically HCV-infected patients; both show a high frequency of accompanying steatosis (10, 40, 41), increased accumulation of carbon 18 monounsaturated fatty acids in the liver (42), mitochondrial dysfunction (43), increased insulin resistance (44) and oxidative stress (45, 46), male-preferential (2) and multicentric occurrence of HCC (47, 48), and the well-differentiated appearance of HCC, including trabecular features and often a "nodule-in-nodule" pattern (47, 48). Thus, it is postulated that the mechanism of steatogenesis and hepatocarcinogenesis we proposed may partially apply to patients with chronic HCV infection. If so, therapeutic interventions to alleviate persistent and excessive PPARα activation might be beneficial in the prevention of HCC. To clarify the exact relationship between PPARα activation and HCV-induced hepatocarcinogenesis in humans, further

experiments using noncancerous liver tissues obtained from HCV-related HCC patients and using mice carrying human PPARα and HCV core protein genes are needed.

In conclusion, we clarified for the first time that persistent and potent PPARα activation is absolutely required for the development of severe steatosis and HCC induced by HCV core protein. In addition, we uncovered paradoxical and specific functions of PPARα in the mechanism of steatogenesis mediated by the core protein. Our results offer clues in the search for novel therapeutic and nutritional management options, especially with respect to neutral lipids, for chronically HCV-infected patients.

Methods

Mice. The generation of HCVcpTg mice and *Ppara*$^{-/-}$ mice was described previously (7, 24, 49). Male HCVcpTg mice and female *Ppara*$^{-/-}$ mice were mated, and F1 mice bearing the HCV core protein gene were intercrossed to produce F2 mice. *Ppara*$^{+/+}$, *Ppara*$^{+/-}$, and *Ppara*$^{-/-}$ mice bearing the HCV core protein gene, designated as *Ppara*$^{+/+}$:HCVcpTg, *Ppara*$^{+/-}$:HCVcpTg, and *Ppara*$^{-/-}$:HCVcpTg mice, in the F4 generation were subjected to serial analyses. Because HCC develops preferentially in male HCVcpTg mice (9), male mice were analyzed. Age-matched male *Ppara*$^{+/+}$ mice without the core protein gene were used as controls. For identifying genotypes, genomic DNA was isolated from mouse tails and amplified by PCR. Primer pairs were designed as described elsewhere: 5′-GCCCACAGGACGTTAAGTTC-3′ and 5′-TAGTTCACGCCGTCCTCCAG-3′ for the HCV core gene (7) and 5′-CAGAGCAACCATCCAGATGA-3′ and 5′-AAACGCAACGTAGAGTGCTG-3′ for the PPARα gene (24). Amplified alleles for HCV core and PPARα genes were 460 and 472 base pairs, respectively. Five mice per cage were fed a routine diet and were kept free of specific pathogens according to institutional guidelines. For the clofibrate treatment experiments, 2-month-old male *Ppara*$^{+/-}$ and *Ppara*$^{+/-}$:HCVcpTg mice were randomly divided into 2 groups (n = 20 in each group) and were fed either a routine diet or one containing 0.05% (w/w) clofibrate (Wako Pure Chemicals Industries) for 24 months. All mice were killed by cervical dislocation before their livers were excised. If a hepatic tumor was present, the tumor was removed and subjected to histological analysis, and the remaining liver tissues were used for biochemical analyses. All animal experiments were conducted in accordance with animal study protocols outlined in the *Guide for the Care and Use of Laboratory Animals* prepared by the National Academy of Sciences and approved by the Shinshu University School of Medicine.

Preparation of nuclear, mitochondrial, and cytosolic fractions. Approximately 400 mg of liver tissue was minced on ice and transferred to 10% (w/v) isolation buffer (250 mM sucrose in 10 mM Tris-HCl [pH 7.4] and 0.5 mM EGTA and 0.1% bovine serum albumin [pH 7.4]). The samples were gently homogenized by 10–20 strokes with a chilled Dounce homogenizer (Wheaton) and loose-fitting pestle. The homogenate was centrifuged at 500 × *g* for 5 min at 4°C. The supernatant was retained, and the resulting pellet was resuspended with isolation buffer and centrifuged at 4,500 *g* for 10 min at 4°C. The pellet fraction was suspended again and centrifuged at 20,000 × *g* for 1 h at 4°C, and the resulting pellet was used as the nuclear fraction. The combined supernatant fractions were centrifuged at 7,800 × *g* for 10 min at 4°C to obtain a crude mitochondria pellet. This pellet was resuspended with isolation buffer, centrifuged at 7,800 × *g* for 10 min at 4°C, and used as the mitochondrial fraction. Finally, all supernatant fractions were collected and centrifuged at 20,000 × *g* for 30 min at 4°C, and the resulting supernatant was used as the cytosolic fraction.

Immunoblot analysis. Protein concentrations were measured colorimetrically with a BCA Protein Assay kit (Pierce). For the analysis of fatty acid–metabolizing enzymes, hepatocyte mitochondrial fractions or whole-liver lysates (20 μg protein) were subjected to 10% SDS-PAGE (16). For analysis of PPARα, nuclear fractions (100 μg protein) were used. For analysis of other proteins, whole lysates or cytosolic fractions (50 μg protein) were subjected to electrophoresis. After electrophoresis, the proteins were transferred to nitrocellulose membranes, which were incubated with the primary antibody and then with alkaline phosphatase-conjugated goat anti-rabbit or anti-mouse IgG. Antibodies against HCV core protein, fatty acid–metabolizing enzymes, CYP4A1, catalase, and PPARα were described previously (9, 16, 24, 50). Antibodies against other proteins were purchased commercially: cytochrome *c* antibody from BD Transduction Laboratories and other antibodies from Santa Cruz Biotechnology. The band intensity was measured densitometrically, normalized to that of actin or histone H1, and subsequently expressed as fold changes relative to that of *Ppara*$^{+/+}$ nontransgenic mice.

Analysis of mRNA. Total liver RNA was extracted using an RNeasy Mini Kit (Qiagen), and cDNA was generated by SuperScript II reverse transcriptase (Gibco BRL). Quantitative RT-PCR was performed using a SYBR green PCR kit and an ABI Prism 7700 Sequence Detection System (Applied Biosystems). The primer pairs used for RT-PCR are shown in Table 2. The mRNA level was normalized to the GAPDH mRNA level and subsequently expressed as fold changes relative to that of *Ppara*$^{+/+}$ nontransgenic mice.

Light microscopy and immunohistochemical analysis. Small blocks of liver tissue from each mouse were fixed in 10% formalin in phosphate-buffered saline and embedded in paraffin. Sections (4 μm thick) were stained with hematoxylin and eosin. For immunohistochemical localization of PCNA and 8-OHdG, other small blocks of liver tissue were fixed in 4% paraformaldehyde in phosphate-buffered saline. Sections (4 μm thick) then were affixed to glass slides and incubated overnight with mouse monoclonal antibodies against PCNA (1:100 dilution; Santa Cruz) or 8-OHdG (1:10 dilution; Japan Institute for the Control of Aging). Sections were immunostained using EnVision+ kit, with 3,3′-diaminobenzidine as a substrate (DAKO). Hepatocytes positive for PCNA or 8-OHdG were examined in 10 randomly selected ×400 microscopic fields per section. Two-thousand hepatocytes were examined for each mouse, and the number of immunostained hepatocyte nuclei was expressed as a percentage.

Assessment of hepatocyte apoptosis. TUNEL assay was performed using a MEBSTAIN Apoptosis Kit II (Medical & Biological Laboratories). Two thousand hepatocytes were examined for each mouse, and the number of TUNEL-positive hepatocytes was expressed as a percentage.

Pulse-label and pulse-chase experiments. Parenchymal hepatocytes were isolated by the modified *in situ* perfusion method (51). After perfusion with 0.05% collagenase solution (Wako), the isolated hepatocytes were washed 3 times by means of differential centrifugation and the dead cells were removed by density-gradient centrifugation at 500 *g* for 3 min at 4°C on Percoll (Amersham Pharmacia Biotech). The live hepatocytes were washed and suspended in William's E medium containing 5% FBS. When the viability of the isolated hepatocytes exceeded 85% as determined by the trypan blue exclusion test, the following experiments were conducted. The isolated hepatocytes were washed twice and incubated in methionine-free medium containing 5% dialyzed FBS for 1 h at 37°C. The medium was replaced with the same medium containing 300 mCi/ml of [^{35}S]methionine (Amersham Pharmacia Biotech). After a 3-h incubation, the labeled medium was exchanged for the standard medium, and the preparation was chased for 3, 6, or 12 h. The labeled cells were washed, homogenized, and centrifuged at 800 *g* for 5 min at 4°C to obtain a crude nucleus pellet. This pellet was resuspended with isolation buffer and centrifuged at 20,000 *g* for 1 h at 4°C to prepare the nuclear fraction. The levels of radioactivity in the homogenates of the pulse-labeled preparations were similar between the transgenic and the nontransgenic mice, which suggested that the [^{35}S]methionine uptake capacity in the former hepatocytes was similar to that in the latter. The nuclear fraction was lysed in RIPA buffer (10 mM Tris-HCl, pH 7.4; 0.2% sodium deoxycholate, 0.2% Nonidet P-40, 0.1% SDS,

0.25 mM PMSF, and 10 mg/ml aprotinin). The lysate was incubated for 3 h at 4°C with purified anti-PPARα antibody. The immune complexes were precipitated with *Staphylococcus aureus* protein A bound to agarose beads. After the precipitates had been washed in RIPA buffer, the labeled proteins were resolved by 10% SDS-PAGE and visualized by autoradiography.

Analysis of fatty acid uptake ability. Assays for fatty acid uptake were carried out according to a method reported by Graulet et al. (52) with minor modifications. Briefly, 3 mice in each group were fasted overnight. Livers were removed quickly, rinsed in ice-cold saline solution, and cut into 500-μm thick slices with an Oxford Vibratome (Oxford Laboratories). Approximately 150 mg of fresh liver (6–8 liver slices) was placed on stainless steel grids positioned in a 25-ml flask equipped with suspended plastic center wells (Kontes) and incubated in RPMI-1640 medium (Sigma-Aldrich) devoid of fatty acids for 2 h at 37°C. The medium was then replaced with fresh RPMI-1640 medium supplemented with an antibiotic-antimycotic cocktail and 0.8 mM [1-^{14}C]palmitic acid (4 mCi/mmol) (American Radiolabeled Chemicals) complexed to BSA (palmitic acid:albumin molar ratio of 4:1). After a 7-h incubation, the medium was collected and slices were washed with 2 ml of saline solution and homogenized in Tris buffer (25 mM Tris-HCl, pH 8.0; 50 mM NaCl). Fatty acid uptake ability was calculated as the sum of palmitic acid converted to CO_2 and ketone bodies with that incorporated into total cellular lipids after incubation. For measurement of CO_2 production by the liver slices, the center wells were placed into scintillation vials containing 4 ml of scintillation cocktail, and radioactivity was counted. For measurement of ketone body generation, aliquots of medium (500 μl) and liver homogenates (250 μl) were treated with ice-cold perchloric acid to make final concentrations of 200 mM and were centrifuged at 3,000 *g* for 20 min at 4°C. Aliquots of the supernatant containing the ketone bodies were introduced into the scintillation vials, and radioactivity was counted. Total cellular lipids were extracted from the liver homogenates according to a modified method developed by Folch et al. (53), collected into scintillation vials, and evaporated to dryness under an air stream; radioactivity was then counted. The experiment was repeated 3 times, and palmitic acid uptake ability was expressed as fold changes relative to that of *Ppara*$^{+/+}$ nontransgenic mice.

Other methods. To determine the hepatic content of lipids and lipid peroxides, lipids were extracted according to a method by Folch et al. (53). Triglycerides and free fatty acids were measured with a Triglyceride E-test kit and a NEFA C-test kit (Wako), respectively. Lipid peroxides (malondialdeyde and 4-hydroxyalkenals) were measured using an LPO-586 kit (OXIS International). Hepatic β-oxidation activity was determined as described previously (16). Hepatic caspase 3 activity was measured as described elsewhere (54). Plasma glucose and insulin levels were determined using a Glucose CII-test kit (Wako) and a mouse insulin ELISA kit (U-type, AKRIN-031; Shibayagi), respectively.

Statistics. Statistical analysis was performed with a 2-tailed Student's *t* test for quantitative variables or with a chi-square test for qualitative variables. Quantitative data are expressed as the mean ± SD. $P < 0.05$ was considered to be statistically significant.

Acknowledgments

We thank Trevor Ralph for editorial assistance and Chikako Tanaka for helpful suggestions.

Received for publication August 13, 2007, and accepted in revised form November 7, 2007.

Address correspondence to: Naoki Tanaka, Department of Metabolic Regulation, Institute on Aging and Adaptation, Shinshu University Graduate School of Medicine, Asahi 3-1-1, Matsumoto 390-8621, Japan. Phone: 81-263-37-2850; Fax: 81-263-37-3094; E-mail: naopi@hsp.md.shinshu-u.ac.jp.

1. Kiyosawa, K., et al. 1990. Interrelationship of blood transfusion, non-A, non-B hepatitis and hepatocellular carcinoma: analysis by detection of antibody to hepatitis C virus. *Hepatology.* **12**:671–675.
2. Kiyosawa, K., et al. 2004. Hepatocellular carcinoma: recent trends in Japan. *Gastroenterology.* **127**(5 Suppl. 1):S17–S26.
3. Tanaka, Y., et al. 2002. Inaugural article: a comparison of the molecular clock of hepatitis C virus in the United States and Japan predicts that hepatocellular carcinoma incidence in the United States will increase over the next two decades. *Proc. Natl. Acad. Sci. U. S. A.* **99**:15584–15589.
4. Okuda, K., Fujimoto, I., Hanai, A., and Urano, Y. 1987. Changing incidence of hepatocellular carcinoma in Japan. *Cancer Res.* **47**:4967–4972.
5. El-Serag, H.B., and Mason, A.C. 1999. Rising incidence of hepatocellular carcinoma in the United States. *N. Engl. J. Med.* **340**:745–750.
6. Shimotohno, K. 2000. Hepatitis C virus and its pathogenesis. *Semin. Cancer Biol.* **10**:233–240.
7. Moriya, K., et al. 1997. Hepatitis C virus core protein induces hepatic steatosis in transgenic mice. *J. Gen. Virol.* **78**:1527–1531.
8. Shintani, Y., et al. 2004. Hepatitis C virus infection and diabetes: direct involvement of the virus in the development of insulin resistance. *Gastroenterology.* **126**:840–848.
9. Moriya, K., et al. 1998. The core protein of hepatitis C virus induces hepatocellular carcinoma in transgenic mice. *Nat. Med.* **4**:1065–1068.
10. Powell, E.E., Jonsson, J.R., and Clouston, A.D. 2005. Steatosis: co-factor in other liver diseases. *Hepatology.* **42**:5–13.
11. Ohata, K., et al. 2003. Hepatic steatosis is a risk factor for hepatocellular carcinoma in patients with chronic hepatitis C virus infection. *Cancer.* **97**:3036–3043.
12. Browning, J.D., and Horton, J.D. 2004. Molecular mediators of hepatic steatosis and liver injury. *J. Clin. Invest.* **114**:147–152.
13. Le, T.H., et al. 2004. The zonal distribution of megamitochondria with crystalline inclusions in nonalcoholic steatohepatitis. *Hepatology.* **39**:1423–1429.
14. Yang, S., Lin, H.Z., Hwang, J., Chacko, V.P., and Diehl, A.M. 2001. Hepatic hyperplasia in noncirrhotic fatty livers: is obesity-related hepatic steatosis a premalignant condition? *Cancer Res.* **61**:5016–5023.
15. Desvergne, B., and Wahli, W. 1999. Peroxisome proliferator-activated receptors: nuclear control of metabolism. *Endocr. Rev.* **20**:649–688.
16. Aoyama, T., et al. 1998. Altered constitutive expression of fatty acid-metabolizing enzymes in mice lacking the peroxisome proliferator-activated receptor α (PPARα). *J. Biol. Chem.* **273**:5678–5684.
17. Staels, B., et al. 1998. Mechanism of action of fibrates on lipid and lipoprotein metabolism. *Circulation.* **98**:2088–2093.
18. Harano, Y., et al. 2006. Fenofibrate, a peroxisome proliferator-activated receptor α agonist, reduces hepatic steatosis and lipid peroxidation in fatty liver Shionogi mice with hereditary fatty liver. *Liver Int.* **26**:613–620.
19. Yeldandi, A.V., Rao, M.S., and Reddy, J.K. 2000. Hydrogen peroxide generation in peroxisome proliferator-induced oncogenesis. *Mutat. Res.* **448**:159–177.
20. Yu, S., Rao, M.S., and Reddy, J.K. 2003. Peroxisome proliferator-activated receptors, fatty acid oxidation, steatohepatitis and hepatocarcinogenesis. *Curr. Mol. Med.* **3**:561–572.
21. Peters, J.M., Cattley, R.C., and Gonzalez, F.J. 1997. Role of PPARα in the mechanism of action of the nongenotoxic carcinogen and peroxisome proliferator Wy-14,643. *Carcinogenesis.* **18**:2029–2033.
22. Fan, C.Y., et al. 1998. Steatohepatitis, spontaneous peroxisome proliferation and liver tumors in mice lacking peroxisomal fatty acyl-CoA oxidase. Implications for peroxisome proliferator-activated receptor α natural ligand metabolism. *J. Biol. Chem.* **273**:15639–15645.
23. Moriya, K., et al. 2001. Oxidative stress in the absence of inflammation in a mouse model for hepatitis C virus-associated hepatocarcinogenesis. *Cancer Res.* **61**:4365–4370.
24. Lee, S.S., et al. 1995. Targeted disruption of the α isoform of the peroxisome proliferator-activated receptor gene in mice results in abolishment of the pleiotropic effects of peroxisome proliferators. *Mol. Cell. Biol.* **15**:3012–3022.
25. Mandard, S., Muller, M., and Kersten, S. 2004. Peroxisome proliferator-activated receptor α target genes. *Cell. Mol. Life Sci.* **61**:393–416.
26. Peters, J.M., et al. 1998. Role of peroxisome proliferator-activated receptor α in altered cell cycle regulation in mouse liver. *Carcinogenesis.* **19**:1989–1994.
27. Tsutsumi, T., et al. 2002. Interaction of hepatitis C virus core protein with retinoid X receptor α modulates its transcriptional activity. *Hepatology.* **35**:937–946.
28. Tanaka, N., et al. 2003. In vivo stabilization of nuclear retinoid X receptor α in the presence of peroxisome proliferator-activated receptor α. *FEBS Lett.* **543**:120–124.
29. Moriishi, K., et al. 2007. Critical role of PA28γ in hepatitis C virus-associated steatogenesis and hepatocarcinogenesis. *Proc. Natl. Acad. Sci. U. S. A.* **104**:1661–1666.
30. Perlemuter, G., et al. 2002. Hepatitis C virus core

protein inhibits microsomal triglyceride transfer protein activity and very low density lipoprotein secretion: a model of viral-related steatosis. *FASEB J.* **16**:185–194.
31. Korenaga, M., et al. 2005. Hepatitis C virus core protein inhibits mitochondrial electron transport and increases reactive oxygen species (ROS) production. *J. Biol. Chem.* **280**:37481–37488.
32. Gomez-Gonzalo, M., et al. 2004. Hepatitis C virus core protein regulates p300/CBP co-activation function. Possible role in the regulation of NF-AT1 transcriptional activity. *Virology.* **328**:120–130.
33. Yu, S., and Reddy, J.K. 2007. Transcription coactivators for peroxisome proliferator-activated receptors. *Biochim. Biophys. Acta.* **1771**:936–951.
34. Spaziani, A., Alisi, A., Sanna, D., and Balsano, C. 2006. Role of p38 MAPK and RNA-dependent protein kinase (PKR) in hepatitis C virus core-dependent nuclear delocalization of cyclin B1. *J. Biol. Chem.* **281**:10983–10989.
35. Diradourian, C., Girard, J., and Pegorier, J.P. 2005. Phosphorylation of PPARs: from molecular characterization to physiological relevance. *Biochimie.* **87**:33–38.
36. Reddy, J.K., Rao, M.S., Azarnoff, D.L., and Sell, S. 1979. Mitogenic and carcinogenic effects of a hypolipidemic peroxisome proliferator, [4-chloro-6-(2,3-xylidino)-2- pyrimidinylthio]acetic acid (Wy-14,643), in rat and mouse liver. *Cancer Res.* **39**:152–161.
37. Rao, M.S., and Reddy, J.K. 1996. Hepatocarcinogenesis of peroxisome proliferators. *Ann. N. Y. Acad. Sci.* **804**:573–587.
38. Genini, D., and Catapano, C.V. 2006. Control of peroxisome proliferator-activated receptor fate by the ubiquitin-proteasome system. *J. Recept. Signal. Transduct. Res.* **26**:679–692.
39. Dharancy, S., et al. 2005. Impaired expression of the peroxisome proliferator-activated receptor alpha during hepatitis C virus infection. *Gastroenterology.* **128**:334–342.
40. de Gottardi, A., et al. 2006. Peroxisome proliferator-activated receptor-alpha and -gamma mRNA levels are reduced in chronic hepatitis C with steatosis and genotype 3 infection. *Aliment. Pharmacol. Ther.* **23**:107–114.
41. Lefkowitch, J.H., et al. 1993. Pathological diagnosis of chronic hepatitis C: a multicenter comparative study with chronic hepatitis B. *Gastroenterology.* **104**:595–603.
42. Moriya, K., et al. 2001. Increase in the concentration of carbon 18 monounsaturated fatty acids in the liver with hepatitis C: analysis in transgenic mice and humans. *Biochem. Biophys. Res. Commun.* **281**:1207–1212.
43. Barbaro, G., et al. 1999. Hepatocellular mitochondrial alterations in patients with chronic hepatitis C: ultrastructural and biochemical findings. *Am. J. Gastroenterol.* **94**:2198–2205.
44. Hui, J.M., et al. 2003. Insulin resistance is associated with chronic hepatitis C virus infection and fibrosis progression [corrected]. *Gastroenterology.* **125**:1695–1704.
45. Kato, J., et al. 2001. Normalization of elevated hepatic 8-hydroxy-2'-deoxyguanosine levels in chronic hepatitis C patients by phlebotomy and low iron diet. *Cancer Res.* **61**:8697–8702.
46. Horiike, S., et al. 2005. Accumulation of 8-nitroguanine in the liver of patients with chronic hepatitis C. *J. Hepatol.* **43**:403–410.
47. Takenaka, K., et al. 1994. Possible multicentric occurrence of hepatocellular carcinoma: a clinicopathological study. *Hepatology.* **19**:889–894.
48. Oikawa, T., et al. 2005. Multistep and multicentric development of hepatocellular carcinoma: histological analysis of 980 resected nodules. *J. Hepatol.* **42**:225–229.
49. Akiyama, T.E., et al. 2001. Peroxisome proliferator-activated receptor-α regulates lipid homeostasis, but is not associated with obesity. *J. Biol. Chem.* **276**:39088–39093.
50. Nakajima, T., et al. 2004. Peroxisome proliferator-activated receptor α protects against alcohol-induced liver damage. *Hepatology.* **40**:972–980.
51. Ni, R., et al. 1994. Fas-mediated apoptosis in primary cultured mouse hepatocytes. *Exp. Cell Res.* **215**:332–337.
52. Graulet, B., Gruffat, D., Durand, D., and Bauchart, D. 1998. Fatty acid metabolism and very low density lipoprotein secretion in liver slices from rats and preruminant calves. *J. Biochem.* **124**:1212–1219.
53. Folch, J., Lees, M., and Sloane Stanley, G.H. 1957. A simple method for the isolation and purification of total lipids from animal tissues. *J. Biol. Chem.* **226**:497–509.
54. Gurtu, V., Kain, S.R., and Zhang, G. 1997. Fluorometric and colorimetric detection of caspase activity associated with apoptosis. *Anal. Biochem.* **251**:98–102.

A New Prognostic System for Hepatocellular Carcinoma Including Recurrent Cases

A Study of 861 Patients in a Single Institution

Takashi Toyama, MD, PhD, Naoki Hiramatsu, MD, PhD,† Takayuki Yakushijin, MD, PhD,† Tsugiko Oze, MD,† Fumihiko Nakanishi, MD, PhD,† Masakazu Yasumaru, MD, PhD,† Kiyoshi Mochizuki, MD, PhD,† Tatsuya Kanto, MD, PhD,† Tetsuo Takehara, MD, PhD,† Akinori Kasahara, MD, PhD,‡ and Norio Hayashi, MD, PhD†*

Objective: To manage hepatocellular carcinoma (HCC) patients surviving for a long term, the treatment strategy for recurrent cancer is as important as that for the initial treatment. However, no prognostic scoring system has been available for patients with HCC recurrence. The purpose of this study was to develop a new staging system for deciding the treatment strategy not only for first-time diagnosed patients but also for recurrent patients.

Methods: A total of 861 cases diagnosed at our single institution from 1993 to 2003 were included. Overall survival was the only end point. The Cox model was used for multivariate analyses.

Results: As of August 2004, 344 cases (59%) had died. Overall median survival time was 41 months. For multivariate Cox regression analysis, independent predictive factors of survival were the number of recurrences, the Child-Pugh score, 3 nodules less than 3 cm and none of vascular invasion, and the α-fetoprotein level. A simple scoring system was thus developed, assigning scores (0/1) to the 4 covariates of the final model. Compared with the other scoring systems, the new scoring system has a greater discriminant ability.

Conclusions: We concluded that our scoring system can serve as a new prognostic system that reflects the spread of HCC, treatment response, and liver function. It should be very useful as the only method which can be applied for patients with recurrence.

Key Words: hepatocellular carcinoma, recurrence, staging system, predictive factor, cox regression analysis

(*J Clin Gastroenterol* 2008;42:317–322)

Received for publication December 6, 2006; accepted May 8, 2007.

From the *Liver Research Center, Rhode Island Hospital/Brown Medical School, Providence, RI; Departments of †Gastroenterology and Hepatology; and ‡General Medicine, Graduate School of Medicine, Osaka University, Osaka, Japan.

The authors declare no conflict of interest.

The authors confirm that there is no financial arrangement from the manufacturer with this study.

Reprints: Takashi Toyama, MD, PhD, Liver Research Center, Rhode Island Hospital/Brown Medical School, 55 Claverick Street, Providence, RI 02903 (e-mail: toyama.takashi@gmail.com).

Recently, various nonsurgical treatment modalities for hepatocellular carcinoma (HCC) have been developed and surgical techniques have been also improved.[1,2] However, HCC with cirrhosis remains one of the diseases that is extremely difficult to manage, because survival in HCC is not predominantly based on the biology of the tumor, but also on the underlying hepatic function. Actually, we need consider 2 distinctive features in planning the HCC treatment from other cancers. First, even if HCC can be completely treated, the residual cirrhotic liver displays a high risk of recurrence, including new primary cancers.[3–5] Second, most options for the treatment of HCC lead to a decrease in the reserved hepatic function. In other words, they take the risk of future liver failure in return for HCC treatment. Taken together, the complexity of these factors makes HCC management difficult.

The prognosis of HCC patients is highly variable and hard to predict, which makes it difficult to effectively treat patients or to design good clinical trials. To provide guides for assessing disease severity and making therapeutic decisions, several staging or prognostic scoring systems for HCC have been proposed: the Cancer of the Liver Italian Program (CLIP) score,[6] BCLC staging,[7] and Japan Integrated Staging (JIS) scoring system,[8] which were produced on the basis of prognostic values. These staging systems can be used for assessing the prognosis of HCC patients as well as the efficiency of therapeutic modalities. Although these systems may be useful for predicting the prognosis of HCC patients at the time of the initial treatment,[9–11] there is considerable doubt about whether these systems are suitable for cases of recurrent cancer, because they cannot distinguish HCC diagnosed for the first time from recurrent HCC. In clinical practice, recurrent HCC patients are encountered 2.5 times more frequently in our institution than first-time HCC patients. Because the development of screening and follow-up programs and the improvement of radiologic techniques have facilitated the recognition of HCC at an earlier

stage,[12,13] it has become possible to repeatedly apply curative treatments.

To manage HCC patients surviving for a long term, preparing the treatment strategy for recurrent cancer becomes more important than that for initial treatment. This makes it important to predict the prognosis of recurrent patients. In other words, every time HCC is diagnosed, the prognostic value should be assessed, and then a treatment strategy should be decided. However, no attempts have been made to include prediction of the prognosis of recurrent HCC patients. The purpose of this article is to propose a new prognostic scoring system, which can be useful for deciding the treatment strategy not only for first-time diagnosed patients but also for recurrent HCC patients.

PATIENTS AND METHODS

Study Population

All (888) consecutive adult patients who were diagnosed as HCC and registered with the Division of Internal Medicine in the Osaka University Hospital between 1993 and 2003, were eligible for this study. Sixteen patients who could not be confirmed as having HCC were excluded. Three patients who underwent liver transplantation were also excluded. Eight patients who had local recurrences within 6 months were excluded because their admissions were not for the recurrent tumor but rather for the residual tumors caused by the insufficient ablation therapy. Thus, 861 patients composed the study population. The patient data were collected with both a survey of original medical records and access to the hospital information system. The patient data set was divided into 2 data sets for a split-sample validation procedure,[14] one set being retrospectively collected patients (n = 578) between September 1, 1993 and December 31, 2001, and the other being prospectively collected patients (n = 283) with the hospital database system between January 1, 2002 and December 31, 2003. The former was used as a training sample to construct a prognostic scoring system; the latter was used as a validation sample for the validation of the generated classification. HCC diagnosis was mainly established by the concomitant finding of 2 imaging techniques (n = 438), showing a nodule with arterial hypervascularization and portal hypovascularization, or by a positive imaging technique, showing hypervascularization associated with elevation of α-fetoprotein (AFP) or protein induced by vitamin K absence II (PIVKA-II) (n = 272). In addition, even if the above-mentioned features were not observed, target biopsy was performed when the findings of ultrasonography were consistent with HCC (n = 151). Details of the treatment modality showed that trans-catheter arterial chemoembolization alone or combined with percutaneous tumor ablation were mainly performed (n = 306 and 301, respectively). The number of patients treated with surgical resection, percutaneous tumor ablation alone, and best supportive care were 46, 188, and 20 respectively.

Statistical Methods

Overall survival was the only end point used in the analysis. It was defined as the time elapsed from the date of diagnosis and either the date of death related to liver disease or the date of the last follow-up information, with the final evaluation conducted on August 31, 2004. Patients lost before the last collection of follow-up information were censored at the time of their last visit. One hundred thirty-one of the 238 censored cases in the training sample were alive at the end of the period, whereas 22 patients had died from other diseases and 85 were lost to follow-up owing to change of residence (n = 21), introduction of a hospital near their residence (n = 50), and unknown reasons (n = 14). Two hundred and two of the 223 censored cases in the validation sample were alive, 3 patients died from other diseases, and 19 cases were loss to follow-up owing to the change of residence (n = 1), introduction of a hospital near their residence (n = 11), and unknown reasons (n = 7). Judging from the data at their last visit, all of the censored samples were considered to be independent of the future value of the hazard for the individual, in other words, they were noninformative censored cases. Figure 1 shows a schematic overview of investigated patients and dropouts for training and validation sample.

The following variables were used for the analysis: age and sex of the patient, date of HCC diagnosis, date of death or of last available information, viral status, the number of HCC recurrences, Child-Pugh score, the largest tumor size, tumor number, vascular invasion, AFP level, and PIVKA-II level. The cut-off levels of continuous variables were chosen on the basis of clinical meaning. For each variable, missing data were not used in the analysis if they accounted for less than 10% of the cases.

Univariate survival curves were estimated using the Kaplan-Meier method[15] and compared by means of the log-rank test.[16] The prognostic impact of the categories was assessed by means of the observed/expected ratio, as described previously.[6] Of the factors affecting patient survival in univariate analysis, baseline predictors were identified by the Akaike information criterion in a stepwise algorithm.[17] Next, a Cox proportional hazard

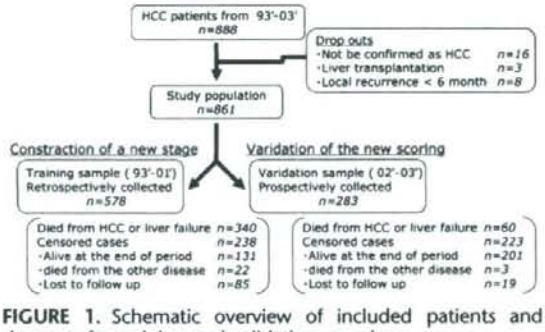

FIGURE 1. Schematic overview of included patients and dropouts for training and validation sample.

regression model was used for multivariate analyses.[18] Proportional hazard assumption was graphically assessed using plots of Log [−Log (survival time)]. Cases with missing values for one or more variables in the model were excluded from multivariate analysis. Treatment was not included in the model because the treatment choice was closely associated with the assessment of prognosis at the time of diagnosis.

Finally, the validity of the generated score was then assessed for the validation sample; a recent sample and a prospectively followed sample. The predictive accuracy of 3 models: this new score system, JIS score system, and CLIP score system was quantified by calculating the concordance index (C-index), which provides the area under the receiver operating characteristics (ROC) curve for the prediction of death at 3 years, as described previously.[19] A C-index of 0.5 indicates that outcomes are completely random, whereas a C-index of 1.0 indicates that the model is a perfect predictor.

All analyses were performed with R's software (R Foundation for Statistical Computing, Austria).[20] $P < 0.05$ was considered statistically significant in all analyses. The results were reported as a hazard ratio with 95% confidence intervals.

RESULTS

As of August 2004, 344 patients (59%) had died. The overall median survival time was 41 months (95% confidence interval, 36 to 46 mo); 1, 3, 5-year survival rates were 86%, 56%, and 35%, respectively. The baseline characteristics of the patients are given in Table 1. The first-time diagnosed HCC, shown as the number of HCC recurrences = 0 in Table 1, amounted to 295 cases, the first recurrence to 185, the second recurrence to 126, the third recurrence to 90, and more than the fourth recurrence to 165. Most cases were in the Child-Pugh A category. The baseline characteristics of the tumor are given in Table 2.

Nine variables were separately found to be associated with the outcome in univariate analysis of 11 variables (as shown in Table 3). Forward stepwise selection by Akaike information criterion was used to identify baseline predictors of 9 variables. Five variables were selected: the Child-Pugh score, the number of tumors, AFP, vascular invasion, and the number of HCC recurrences. To better reflect the treatment response, we combined 2 factors to create a single factor: we replaced "the number of tumors and vascular invasion" with "3 nodules less than 3 cm and none of vascular invasion, or not," called the tumor factor. This was done because the criterion "3 nodules less than 3 cm" reflects the possibility of complete response to ablation treatment[21] and was useful in the current clinical setting. We finally chose 4 factors for a new prognostic classification: the Child-Pugh score, tumor factor, AFP, and the number of HCC recurrences. These 4 covariates showed correlation with survival in the Cox regression analysis.

Each covariate selected by means of forward stepwise methods was divided into 2 categories to derive a simple scoring system. The cut-off levels were chosen where each estimated regression coefficient of the final Cox model was almost the same, that is, we made the relative prognostic weight of covariates the same, around 2 each (shown as in Table 4). A new scoring system was derived to assign scores (0/1) to each covariate of the final model as shown in Table 4. This classification was relatively easy to calculate by summing up each individual score of the 4 covariates. Five risk groups were constituted according to the score distribution. The survival curve of 578 patients calculated by the Kaplan-Meier method is shown in Figure 2A.

We assessed the new score system for 283 patients for the validation sample; prospectively obtained from 2002 to 2003 in Figure 2B. This result validated our scoring system and showed that it can be applied in today's clinical setting. This applicability to the present-day situation is very important, because diagnostic and

TABLE 1. Characteristics of Patients

Variables	Training Sample No. Patients	Validation Sample No. Patients
Median age, y (range)	64 (21-85)	67 (35-83)
Male (%)	425 (73.5)	192(67.8)
Cause of parenchymal disorder		
HBV/HCV/HB + HC	54/486/10	27/227/4
Alcoholic	8	10
Others	20	15
Child-Pugh score (unknown = 1)		
5-6 (A)/7-9 (B)/10-12 (C)	342/218/18	192/79/11
Number of HCC recurrence		
0/1/2/3/≥4	201/123/88/62/104	94/62/38/28/61

HBV indicates Hepatitis B virus; HCV, Hepatitis C virus.

TABLE 2. Characteristics of the Tumor

	Training Sample No. Patients	Validation Sample No. Patients
Number of tumor		
1/2/3/4/≥5	186/113/57/36/186	112/56/28/18/69
Largest size of tumor (cm)		
≤2.0/2.1-3.0/3.1-5.0/≥5.1	270/163/91/54	128/82/44/29
Vascular invasion		
Yes/no	534/44	266/17
Tumor factor [3 nodule less than 3 cm, vascular invasion (−)]		
Yes/no	285/293	159/124
AFP category (ng/mL)		
$\leq 10/10\text{-}10^2/10^2\text{-}10^3/ > 10^3$	137/230/129/82	65/108/70/40
PIVKA-II (mAU/mL) (unknown = 81)		
$\leq 10^2/10^2\text{-}10^3/10^3\text{-}10^4/ > 10^4$	327/118/64/27	110/58/20/14

TABLE 3. Univariate Analysis of Clinical Findings for Survival

Variables	No. Patients	O/E Ratio	*P*	DOF
Sex			0.00168	1
Male/female	425/153	1.11/0.73		
Age			0.00284	3
≤50/50-60/60-70/≥70	37/118/291/132	0.53/0.87/1.19/0.86		
Etiology			0.147	3
HCV/HBV/HB + HC/the others	486/54/10/28	1.03/0.9/1.38/0.54		
Number of HCC recurrence			< 0.0001	4
0/1/2/3/≥4	201/123/88/62/104	0.57/0.93/1.2/1.33/2.1		
Child-Pugh stage			< 0.0001	2
A/B/C	342/218/18	0.75/1.49/2.72		
Largest size of tumor (cm)			0.00467	3
≤2.0/2.1-3.0/3.1-5.0/≥5.1	270/163/91/54	0.86/1.06/1.16/1.65		
Number of tumor			< 0.0001	4
1/2/3/4/≥5	186/113/57/36/186	0.52/0.95/0.97/1.04/2.03		
Vascular invasion			< 0.0001	1
Yes/no	534/44	0.93/3.78		
Tumor factor [3 nodules less than 3 cm, vascular invasion (−)]			< 0.0001	1
Yes/no	285/293	0.67/1.53		
AFP (ng/mL)			< 0.0001	3
$\leq 10/10\text{-}10^2/10^2\text{-}10^3/>10^3$	137/230/129/82	0.56/0.95/1.2/2.19		
PIVKA-II (mAU/mL)			< 0.0001	3
$\leq 10^2/10^2\text{-}10^3/10^3\text{-}10^4/>10^4$	327/118/64/27	0.76/1.34/1.8/3.65		

DOF indicates degree of freedom; O/E ratio, observed/expected ratio; HBV, Hepatitis B virus; HCV, Hepatitis C virus.

therapeutic procedures for HCC have been improved over recent years.

Finally, the prognostic ability of the new scoring system was compared with CLIP score system and the JIS score system. Kaplan-Meier survival curves were shown in Figs. 2C, D). In addition, the predictive accuracy of 3 models was quantified by calculating a C-index, which provides the area under the ROC curve (as shown in Fig. 3). CLIP stage and JIS scoring had a C-index of 7.05 and 6.93, respectively. This new scoring system had a C-index of 7.23. Our scoring system could discriminate the survival most precisely among them.

DISCUSSION

This article revealed that the number of HCC recurrences is a prognostic factor as well as the reserved liver function and the spreading of HCC, and we have proposed a new scoring system, comprised of 4 parameters: the number of HCC recurrences, the Child-Pugh score, the tumor factor of "3 nodules less than 3 cm and none of vascular invasion," and the AFP level. Each of these parameters has so far been reported to affect patient survival. The occurrence of HCC recurrence reflects disease progression.[3–5] The Child-Pugh score is a well-recognized prognostic variable and reflects reserved liver

TABLE 4. New Scoring System

Variables	Score 0	Score 1	RR
Number of HCC recurrence (n = 578)	0 or 1 (n = 324)	≥2 (n = 254)	2.26
Child-Pugh score (n = 578)	5–7 (n = 486)	≥8 (n = 92)	2.25
Tumor factor (n = 578)	Yes (n = 285)	No (n = 293)	1.90
AFP category (ng/ml) (n = 578)	≤1000 (n = 496)	≥1001 (n = 82)	2.08

RR indicates risk ratio of Score 1 compared with Score 0, assessed by multivariate analysis.

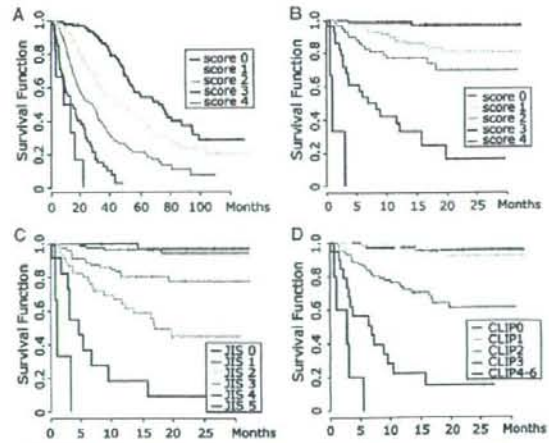

FIGURE 2. Kaplan-Meier–estimated survival curves. A, By our new scoring system in training samples. B, By our new scoring system in validation samples. C, By the CLIP score system in validation samples. D, By the JIS score system in validation samples.

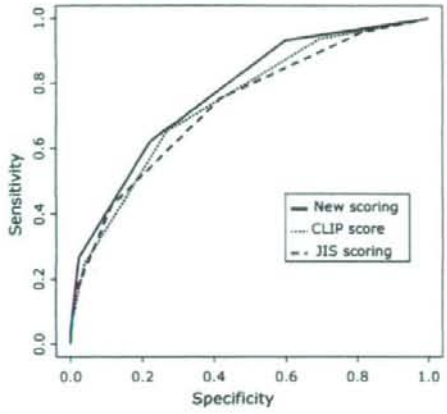

FIGURE 3. Discriminatory ability for the prediction of death at 3 years, evaluated by receiver operating characteristics curves of the new scoring, CLIP, and JIS staging systems.

function.[6,7] The criterion of 3 nodules less than 3 cm is related to the treatment response. Ablation therapy is highly effective for tumors smaller than 3 cm, achieving complete responses of around 80% to 100%.[22] The achievement of a complete and sustained response is an independent prognostic value.[23] AFP is also a well-recognized prognostic variable, and reflects the degree of cellular differentiation and the spreading of the tumor.[24] In the present study, these parameters were independent predictors of survival actually. Elevation of each parameter indicates the progression of HCC. As a result, this new scoring system reflects the spreading of HCC, the response to treatment, and the reserved liver function. In addition, our system is based on not pathologic but easily obtainable and reproducible clinical information. Therefore, this scoring system should be useful in many clinical settings.

A high possibility of recurrence is one of the major characteristics of HCC. Recurrences from either intrahepatic metastasis or de novo HCC exceed 50% at 3 years, even with hepatic resection as curative therapy.[3–5] The more the HCC recurs, the more the prognosis deteriorates because of treatment-induced liver damage and/or tumor progression. In clinical settings, it is very important to carefully follow HCC patients to detect recurrence as early as possible. More and more patients have been able to be frequently treated for recurrent HCC and prolong their survival. What is needed is a treatment strategy based on appropriate cancer staging systems for not only first-time diagnosed HCC but also for recurrent HCC. However, there has been no study reported on the prognosis of recurrent patients. Here, we first showed recurrence to be a prognostic factor with a Cox regression model, and furthermore developed a new scoring system to predict the prognosis of HCC patients including recurrent HCC patients.

What is the problem with applying the other staging systems for the recurrent cases? All of the following staging systems: the CLIP score system,[6] BCLC staging[7] and JIS scoring system[8] were derived from the analysis for first-time diagnosed HCC and were applied only at the initial treatment. Because hypothetical population is different between first-time HCC patients and all HCC patients, their baseline predictors for survival differ from the new scoring system. Indeed, the distributions of both the number of tumor and the largest size of HCC are significantly different between first-time HCC cases and all HCC patients in our cohort (data not shown). As a result, JIS system and CLIP score system may have poor stratification of survival. The goal of cancer staging is to separate patients into different groups on the basis of their predicted survival to help determine the most appropriate treatment modality. Therefore, it is unreasonable to apply their systems for recurrent HCC patients.

Although further evaluation is needed, this scoring system can be useful for conducting interventional trials. With the spread of routine screening and follow-up, the number of recurrent HCC patients can increase. More effective strategies to treat recurrent patients will be needed. In addition, a new modality of treatment will be necessary for HCC management, particularly for score 2 and 3 patients. Interventional trials may be needed to determine the most appropriate therapy for the patients in each group. This scoring system, because of good incorporation between prognosis estimation and potential treatment advances, may be useful for planning and evaluating interventional trials. It would allow us to follow a well-established treatment schedule and select the best treatment modality for each patient when managing long-term–surviving HCC patients.

REFERENCES

1. Llovet JM, Beaugrand M. Hepatocellular carcinoma: present status and future prospects. *J Hepatol*. 2003;38(suppl 1):S136–S149.
2. Befeler AS, Di Bisceglie AM. Hepatocellular carcinoma: diagnosis and treatment. *Gastroenterology*. 2002;122:1609–1619.
3. Ikeda K, Saitoh S, Tsubota A, et al. Risk factors for tumor recurrence and prognosis after curative resection of hepatocellular carcinoma. *Cancer*. 1993;71:19–25.
4. Adachi E, Maeda T, Matsumata T, et al. Risk factors for intrahepatic recurrence in human small hepatocellular carcinoma. *Gastroenterology*. 1995;108:768–775.
5. Arii S, Yamaoka Y, Futagawa S, et al. Results of surgical and nonsurgical treatment for small-sized hepatocellular carcinomas: a retrospective and nationwide survey in Japan. The Liver Cancer Study Group of Japan. *Hepatology*. 2000;32:1224–1229.
6. The Cancer of the Liver Italian Program (CLIP) investigators. A new prognostic system for hepatocellular carcinoma: a retrospective study of 435 patients. *Hepatology*. 1998;28:751–755.
7. Llovet JM, Bru C, Bruix J. Prognosis of hepatocellular carcinoma: the BCLC staging classification. *Semin Liver Dis*. 1999;19:329–338.
8. Kudo M, Chung H, Osaki Y. Prognostic staging system for hepatocellular carcinoma (CLIP score): its value and limitation, and a proposal for a new staging system, the Japan Integrated Staging Score (JIS score). *J Gastroenterol*. 2003;38:207–215.

9. Chevret S, Trinchet JC, Mathieu D, et al. A new prognostic classification for predicting survival in patients with hepatocellular carcinoma. Groupe d'Etude et de Traitement du Carcinome Hepatocellulaire. *J Hepatol*. 1999;31:133–141.
10. The Cancer of the Liver Italian Program (CLIP) investigation. Prospective validation of the CLIP score: a new prognostic system for patients with cirrhosis and hepatocellular carcinoma. *Hepatology*. 2000;31:840–845.
11. Kudo M, Chung H, Haji S, et al. Validation of a new prognostic staging system for hepatocellular carcinoma: the JIS score compared with the CLIP score. *Hepatology*. 2004;40:1396–1405.
12. Taouli B, Losada M, Holland A, et al. Magnetic resonance imaging of hepatocellular carcinoma. *Gastroenterology*. 2004;127: S144–S152.
13. Baron RL, Brancatelli G. Computed tomographic imaging of hepatocellular carcinoma. *Gastroenterology*. 2004;127:S133–S143.
14. Van Houwelingen JC, Le Cessie JC. Predictive value of statistical models. *Stat Med*. 1990;9:1303–1325.
15. Kaplan E, Meier P. Nonparametric estimation from incomplete observations. *J Am Stat Assoc*. 1958;53:457–481.
16. Peto R, Peto J. Asymptomatically efficient rank invariant test procedure. *J Roy Stat*. 1972;135:185–206.
17. Akaike H. A new look at the statistical model identification. *IEEE Trans Automatic Control*. 1974;AC-19:716–723.
18. Cox DR. Regression models and life tables. *J R Stat Soc*. 1972; B34:187–220.
19. Kim HL, Seligson D, Liu X, et al. Using protein expressions to predict survival in clear cell renal carcinoma. *Clin Cancer Res*. 2004; 10:5464–5474.
20. Development Core Team. R: *A language and environment for statistical computing*. Vienna, Austria: R Foundation for Statistical Computing; 2004.
21. Vilana R, Bruix J, Bru C, et al. Tumor size determines the efficacy of percutaneous ethanol injection for the treatment of small hepatocellular carcinoma. *Hepatology*. 1992;16:353–357.
22. Bruix J, Llovet JM. Prognostic prediction and treatment strategy in hepatocellular carcinoma. *Hepatology*. 2002;35:519–524.
23. Livraghi T, Giorgio A, Marin G, et al. Hepatocellular carcinoma and cirrhosis in 746 patients: long-term results of percutaneous ethanol injection. *Radiology*. 1995;197:101–108.
24. Nomura F, Ohnishi K, Tanabe Y. Clinical features and prognosis of hepatocellular carcinoma with reference to serum alpha-fetoprotein levels. Analysis of 606 patients. *Cancer*. 1989;64: 1700–1710.

European Journal of Pharmacology 604 (2009) 87–92

Contents lists available at ScienceDirect

European Journal of Pharmacology

journal homepage: www.elsevier.com/locate/ejphar

Cardiovascular Pharmacology

Administration of angiotensin II, but not catecholamines, induces accumulation of lipids in the rat heart

Makiko Hongo [a], Nobukazu Ishizaka [a,*], Kyoko Furuta [a], Naoya Yahagi [b], Kan Saito [a], Ryota Sakurai [a], Gen Matsuzaki [a], Kazuhiko Koike [c], Ryozo Nagai [a]

[a] Department of Cardiovascular Medicine, University of Tokyo, Graduate School of Medicine, Hongo 7-3-1, Bunkyo-ku, Tokyo 113-8655, Japan
[b] Department of Diabetes and Metabolic Disease, University of Tokyo, Graduate School of Medicine, Hongo 7-3-1, Bunkyo-ku, Tokyo 113-8655, Japan
[c] Department of Infectious Disease, University of Tokyo, Graduate School of Medicine, Hongo 7-3-1, Bunkyo-ku, Tokyo 113-8655, Japan

ARTICLE INFO

Article history:
Received 9 May 2008
Received in revised form 20 November 2008
Accepted 3 December 2008
Available online 10 December 2008

Keywords:
Angiotensin II
Lipid accumulation
Lipotoxicity
Gene expression

ABSTRACT

Accumulation of lipids in the heart may cause cardiac dysfunction in various disorders, such as obesity and diabetes. In the current study, we have investigated whether administration of angiotensin II or norepinephrine induces accumulation of lipids and/or changes in the expression of genes related to lipid metabolism in the rat heart. Lipid deposition was found in myocardial, vascular wall, and perivascular cells of the angiotensin II-infused rat heart, and superoxide generation was increased in these lipid-positive cells. By contrast, intracardiac lipid deposition was not found in the heart of norepinephrine-induced hypertensive rats. Triglyceride content in the heart tissue of angiotensin II-infused rats increased more than 3-fold as compared with untreated controls. Losartan completely, but hydralazine only partially, suppressed the angiotensin II-induced intracardiac lipid deposition and increase in tissue triglyceride content. Administration of angiotensin II upregulated the mRNA expression of sterol regulatory element-binding protein-1c and fatty acid synthase, but downregulated that of uncoupling protein 2 and 3, in a manner dependent on the angiotensin AT_1 receptor. Collectively, these results suggest that angiotensin II may be involved in modulating both intracardiac lipid content and lipid metabolism-related gene expression, in part via an angiotensin AT_1 receptor-dependent and pressor-independent mechanism.

1. Introduction

Accumulation of lipids in non-adipose tissues can occur in certain disease conditions, including aging, over-nutrition, obesity, and diabetes, and may play a crucial role in the pathogenesis of tissue damage (Schaffer, 2003), a phenomenon referred to as lipotoxicity (Unger, 2002). Inappropriate accumulation of free fatty acids and neutral lipids can also be observed in the myocardium; this accumulation may result in both functional and morphological damage, such as systolic and/or diastolic dysfunction of the left ventricle (Chiu et al., 2005, Zhou et al., 2000), ventricular wall hypertrophy (Finck et al., 2003, Horiuchi et al., 1993), and interstitial fibrosis (Lee et al., 2004). In previous studies, we found that administration of angiotensin II to rats causes deposition of lipids in tubular epithelial and vascular wall cells in the kidney (Ishizaka et al., 2006, Saito et al., 2005), where cellular proliferation may be promoted. In the current study, we have investigated whether administration of two different pressor agents, angiotensin II and a catecholamine, causes intracardiac accumulation of lipids, and modulates the expression of genes related to lipid metabolism.

2. Materials and methods

2.1. Animal models

The experiments were performed in accordance with the guidelines for animal experimentation approved by the Animal Center for Biomedical Research, Faculty of Medicine, University of Tokyo. Angiotensin II-induced hypertension was induced in male Sprague-Dawley rats (250 to 300 g) by subcutaneous implantation of an osmotic minipump (Alza Pharmaceutical) as described previously (Ishizaka et al., 1997). Briefly, Val^5-angiotensin II (Sigma Chemical) was infused at doses of 0.7 mg/kg/day. Norepinephrine (Sigma Chemical) was infused at a dose of 2.8 mg/kg/day for 7 days using the same system. In some angiotensin II-infused rats, angiotensin AT_1 receptor antagonist, losartan (25 mg/kg/day), or the nonspecific vasodilator, hydralazine (15 mg/kg/day) (Sigma Chemical), both of which normalized the blood pressure of angiotensin II-infused rats, was given in the drinking water (Ishizaka et al., 2002).

* Corresponding author. Department of Cardiovascular Medicine, University of Tokyo, Graduate School of Medicine, Hongo 7-3-1, Bunkyo-ku, Tokyo 113-8655, Japan. Tel.: +81 3 3815 5411x3016; fax: +81 3 3974 2236.
E-mail address: nobuishizka-tky@umin.ac.jp (N. Ishizaka).

0014-2999/$ – see front matter © 2009 Elsevier B.V. All rights reserved.
doi:10.1016/j.ejphar.2008.12.006

Table 1
Oligonucleotide primers used in this study

Gene	GenBank no.	Forward primer	Reverse primer
PPAR-α	NM_013196	GTGGCTGCTATAATTTGCTG	TGAAGGAGTTTTGGGAAGAG
PPAR-γ	NM_013124	ATCAGCTCTGTGGACCTCTC	AGGCTCTACTTTGATCGCAC
SREBP-1c	XM_213329	CTGATGGAGACAGGGAGTTC	ATCACCACGGCTGTCAGT
FAS	M76767	CTGGAACGTGAACATGATCT	TTCACCAGCAGGATACTCAG
HMG-CoA reductase	NM_013134	GACACTTACAATCTGTATGATG	CTTGGAGAGGTAAAACTGCCA
CPT-1	NM_031559	ATCGACCGCCATCTCTTC	CTCAAAGTCAAAGAGCTCCAC
CPT-2	NM_012930	TGACCAAAGAAGCAGCGAT	TTGTGGTTCATCTGCTGGTA
DGAT-1	NM_053437	TCTTCCTACCGGGATGTCAATC	TCCCTGCAGACACAGCTTTG
PGC-1α	AY237127	TCATTACCTACCGTTACACCT	CATACTTGCTCTTGGTGGAA
UCP2	BC062230	TGGTCGGAGATACCAGAG	GTCTGTCATGAGGTTGGCT
UCP3	AF035973	GTCCGATTTCAAGCCATGAT	CTTGTGATGTTGGGCCAAGT
Nox1	MN_053683	TGGACGAATTAGGCAAACCG	TTGGGGTGGGCAGTAGCTAT
Nox4	AY027527	AACACTGGTGAAGATTTGC	CTGAGGGATGATTGATTACTG
GAPDH	NM_017008	TGAACGGGAAGCTCACTGG	TCCACCACCCTGTTGCTGTA

PPAR, peroxisome proliferator-activated receptor; SREBP, sterol regulatory element-binding protein; FAS, fatty acid synthase; HMG-CoAR, 3-hydroxy-3-methylglutaryl coenzyme A reductase; CPT, carnitine palmitoyltransferase; DGAT, diacylglycerol acyltransferase; PGC, PPAR-γ coactivator; UCP, uncoupling protein; and GAPDH, glyceraldehyde-3-phosphate dehydrogenase.

2.2. Measurement of lipid contents in the serum and the heart

Serum levels of total cholesterol, triglycerides, and nonesterified fatty acid were measured by enzymatic methods (SRL). Contents of triglycerides, total cholesterol, and free cholesterol in the heart tissue were measured from homogenate extracts by enzymatic colorimetric determination using Triglyceride-E Test, Cholesterol-E Test, and Free cholesterol-E Test Wako, respectively (Wako Pure Chemicals).

2.3. Histological analysis

Oil red O staining was performed on sections of unfixed, freshly frozen heart samples (3 μm in thickness). The areas of lipid deposition were calculated by using the image analysis software, Photoshop (Adobe), and semiquantification of the lipid deposition was performed as described elsewhere (Ishizaka et al., 2006). Staining with the oxidative fluorescent dye dihydroethidium (DHE) was performed as described previously (Saito et al., 2004). Images were obtained with a fluorescent microscope BX51 (Olympus), and the fluorescence intensity, obtained from at least five fields for each section, was presented as the percentage of that of untreated control.

2.4. Western blot analysis

Western blot analysis was performed as described previously (Aizawa et al., 2000). Antibodies against total and phosphorylated forms AMP-activated protein kinase (Cell Signaling), sterol regulatory element-binding protein (SREBP)-1 (Santa Cruz Biotechnology), SREBP-2 (Santa Cruz Biotechnology), ATP-binding cassette transporter subfamily A1 (ABCA1) (Novus Biologicals), scavenger receptor class B type 1 (SR-B1) (Novus Biologicals), and mitochondrial superoxide dismutase (mt SOD) (Upstate) were used at a dilution of 1/1000.

2.5. Real time reverse transcription-polymerase chain reaction (RT-PCR)

Expression of lipid metabolism-related gene mRNA was analyzed by real time quantitative PCR performed by LightCycler together with hybriprobe technology (Roche Diagnostics). Expression of target genes was normalized to the mRNA expression of endogenous control, glyceraldehyde-3-phosphate dehydrogenase (GAPDH). The target genes were as follows: peroxisome proliferator-activated receptor (PPAR)-α (Nihon Gene Research Lab's Inc., Sendai, Japan), PPAR-γ, SREBP-1c, fatty acid synthase (FAS), 3-hydroxy-3-methylglutaryl coenzyme A reductase (HMG-CoAR), carnitine palmitoyltransferase (CPT)-1, CPT-2, diacylglycerol acyltransferase (DGAT)-1, PPAR-γ coactivator (PGC)-1α, uncoupling protein (UCP)2, UCP3, Nox1, and Nox4. The forward and backward primers used are described in Table 1.

2.6. Statistical analysis

Data are expressed as the mean ± S. E. M. We used ANOVA followed by a multiple comparison test to compare raw data, before expressing the results as a percentage of the control value using the statistical analysis software StatView ver. 5.0 (SAS Institute). A value of $P<0.05$ was considered to be statistically significant.

3. Results

3.1. Characteristics of experimental animals

The hemodynamic parameters in each group have been reported elsewhere (Aizawa et al., 2000). Angiotensin II and norepinephrine elevated the blood pressure to a similar extent, and both hydralazine and losartan completely suppressed the blood pressure elevation induced by angiotensin II. Angiotensin II, but not norepinephrine, significantly increased the serum levels of triglycerides and non-esterified fatty acids, and these increases were inhibited by losartan, but not by hydralazine (Fig. 1A–C).

3.2. Tissue contents of lipids

The tissue content of triglycerides, total cholesterol, and free cholesterol was found to be increased in the heart of angiotensin II-

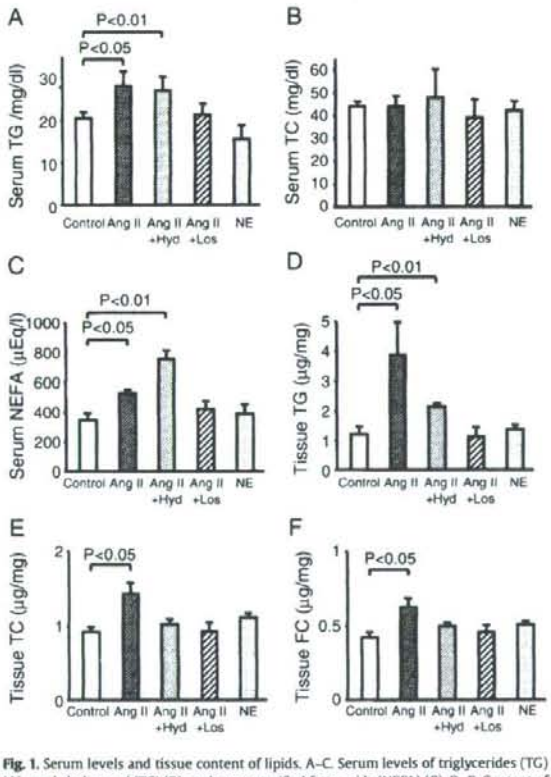

Fig. 1. Serum levels and tissue content of lipids. A–C. Serum levels of triglycerides (TG) (A), total cholesterol (TC) (B), and non-esterified fatty acids (NEFA) (C). D–E. Content of triglycerides (D), total cholesterol (E), free cholesterol (FC) (F) in the heart tissue. Shown in a summary of data from 4–6 rats in each group. Ang II, angiotensin II; Hyd, hydralazine; Los, losartan; and NE, norepinephrine.

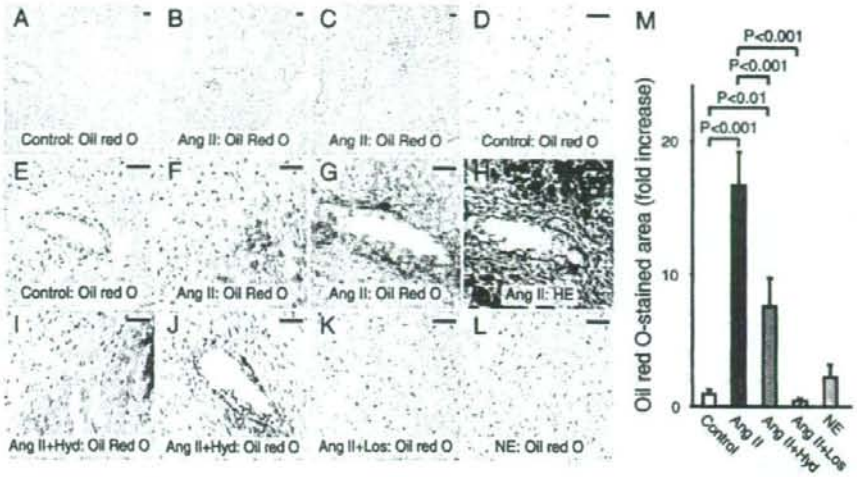

Fig. 2. Accumulation of lipids in the heart. A, D, E. Heart section from a control rat. B, C, F–H. Heart sections from angiotensin II (Ang II)-infused rats. I, J. Heart section from a rat given both angiotensin II and hydralazine (Hyd). K. Heart section from a rat given both angiotensin II and losartan (Los). L. Heart section from a rat given norepinephrine (NE). F and G are serial sections. A–G, I–L. Oil red O staining. H. Hematoxylin eosin (HE) staining. Lipid droplets were not observed in the myocardium or vascular regions (A, D, E) of control rats. Lipid droplets were present in both the myocardium (B, C, F) and perivascular regions (G) in the heart of angiotensin II-infused rats. Lipid droplets in the myocardium (I) and perivascular regions (J) were observed in the heart of rats given both angiotensin II and hydralazine, but not in the heart of rats given angiotensin II plus losartan (K) or those given norepinephrine (L). Original magnification, ×100 (A–C), and ×200 (D–L). Scale bars indicate 50 μm. M. Semiquantification of the oil red O-stained area. Shown is a summary of data from 5–7 experiments in each group.

infused rats, but not norepinephrine-infused rats (Fig. 1). Hydralazine only partially suppressed the angiotensin II-induced increase in intracardiac triglyceride content, but it completely suppressed the increase in intracardiac total cholesterol and free cholesterol content (Fig. 1D–F). Losartan suppressed the angiotensin II-induced increase in all three lipid fractions tested. Administration of losartan alone or hydralazine alone did not significantly alter the lipid content of the heart (losartan: triglycerides, 1.53±0.12 μg/mg, $n=4$; total cholesterol, 1.16±0.07 μg/mg, $n=3$; free cholesterol, 0.53±0.04 μg/mg, $n=4$; hydralazine: triglycerides, 1.40±0.14 μg/mg, $n=4$; total cholesterol, 1.09±0.14 μg/mg, $n=4$; free cholesterol, 0.43±0.04 μg/mg, $n=5$).

3.3. Staining for lipids

Oil red O staining of heart sections showed no apparent lipid deposition in the heart of untreated rats (Fig. 2A, D, E). By contrast, accumulation of oil red O-stainable lipid was observed in the myocardium as well as the arterial wall of angiotensin II-infused rats (Fig. 2B, C, F, G). In the angiotensin II-infused rat heart, lipid accumulation was also observed in perivascular regions, especially where remodeling of perivascular regions was apparent (Fig. 2G, H), and in granulation regions (data not shown). Lipid deposition remained present in the heart when angiotensin II-infused rats were concomitantly treated with hydralazine (Fig. 2I, J). On the other hand, lipid deposition was not apparent, or was very minor when present, in heart sections from rats treated with both angiotensin II and losartan or from rats treated with norepinephrine infusion (Fig. 2K, L). Semiquantitative measurements of the oil red O-stained areas are summarized in Fig. 2M.

3.4. Co-localization of lipid deposition and superoxide

As compared with untreated controls, DHE staining-positive signals were increased in the heart of angiotensin II-infused rats, and

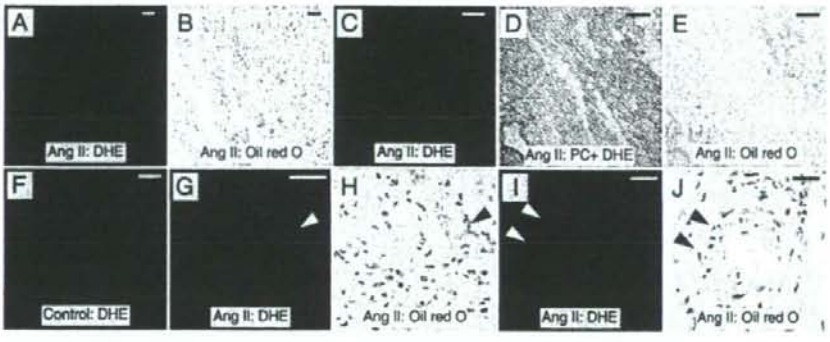

Fig. 3. Lipid and superoxide staining of the heart section. A–E, F–J. Heart sections from angiotensin (Ang) II-infused rats. F. Heart section from a control rat. A, C, F, G, I Dihydroethidium (DHE) staining. D. Phase contrast (PC) microscopic image overlaid with DHE staining image. B, E, H, J. Oil red O staining. C and D are the same section. C (=D)–E, G–H, and I–J are serial sections. Some cells with intense DHE staining (arrowheads in G and I) contained lipid deposits (arrowheads in H and J). Original magnification, ×100 (A–C), ×200 (C–H), and ×400 (I, J). Scale bars indicate 50 μm.

Table 2
mRNA levels of genes related to lipid metabolism

Gene	Control (n=6)	Ang II (n=6)	P	Ang II+Hyd (n=5)	P	Ang II+Los (n=6)	P	NE (n=7)	P
PPAR-α	1±0.17	1.88±0.34	0.030	2.99±0.64	0.005	1.41±0.20	0.080	2.00±0.18	0.001
PPAR-γ	1±0.17	3.30±0.98	0.019	4.25±1.13	0.032	0.83±0.09	0.19	3.56±0.44	<0.001
SREBP-1c	1±0.24	3.66±1.02	0.008	2.67±0.96	0.039	0.71±0.12	0.14	0.77±0.17	0.21
FAS	1±0.17	2.97±0.32	<0.001	3.46±1.00	<0.001	1.30±0.17	0.18	1.28±0.13	0.18
HMG-CoA reductase	1±0.20	2.29±0.30	<0.001	2.50±0.66	0.009	0.99±0.23	0.49	0.98±0.33	0.48
CPT-1	1±0.06	0.55±0.09	<0.001	1.08±0.29	0.395	0.82±0.15	0.154	0.16±0.03	<0.001
CPT-2	1±0.04	0.63±0.06	<0.001	0.67±0.10	<0.001	0.66±0.06	<0.001	0.67±0.05	<0.001
DGAT-1	1±0.04	1.20±0.12	0.071	0.58±0.18	0.003	0.60±0.04	<0.001	0.87±0.12	0.14
PGC-1α	1±0.09	0.52±0.06	<0.001	0.59±0.18	<0.005	0.94±0.18	0.395	1.34±0.31	0.17
UCP2	1±0.08	0.51±0.08	<0.001	0.39±0.08	<0.001	0.80±0.09	0.055	1.53±0.79	0.276
UCP3	1±0.06	0.75±0.09	0.020	0.50±0.11	<0.001	0.74±0.14	0.037	2.10±0.49	0.038
Nox1	1±0.21	3.31±0.61	0.006	4.87±1.82	0.026	0.90±0.19	0.378	1.17±0.42	0.367
Nox4	1±0.21	5.25±2.22	0.047	0.72±0.10	0.093	1.17±0.12	0.199	1.17±0.14	0.206

P values are versus untreated control. Ang II, angiotensin II; Hyd, hydralazine; Los, losartan; and NE, norepinephrine. Other abbreviations were same as Table 1.

semiquantitative measurements showed that the DHE-stained area was significantly greater after angiotensin II infusion (control 100±37%, $n=5$, versus angiotensin II 342±125%, $n=5$; $P<0.05$). In the heart of angiotensin II-infused rats, some myocardial cells that had increased superoxide staining were found to be positive for lipid deposition (lower magnification in Fig. 3A, B, and higher magnification in Fig. 3C–D). Similarly, some vascular wall and perivascular cells with increased superoxide staining were found to contain lipid deposits (Fig. 3G–J).

3.5. Regulation of genes related to lipid metabolism

Next, we examined the expression of lipid metabolism-related genes after infusion of the pressor agents (Table 2). mRNA expression of PPAR-α, PPAR-γ, SREBP-1c, FAS, and HMG-CoAR was found to be increased in the heart of rats that received angiotensin II infusion. Of the genes tested, mRNA expression of PPAR-α and PPAR-γ was also increased in the heart of the norepinephrine-infused rat. The expression of PGC-1α, UCP2 and UCP3 was decreased after angiotensin II infusion, but not after norepinephrine infusion. The angiotensin II-induced regulation of these genes (PPAR-α, PPAR-γ, SREBP-1c, FAS, HMG-CoAR, PGC-1α, UCP2, and UCP3) was suppressed by losartan, but not by hydralazine. On the other hand, mRNA expression of CPT-1 and CPT-2 was downregulated by angiotensin II. We found that the angiotensin II-induced CPT-1 downregulation was suppressed by depressor agents, and that norepinephrine also downregulated CPT-1 mRNA expression; therefore, the angiotensin II-induced CPT-1 mRNA downregulation might be induced by hypertension per se. Angiotensin II increased the mRNA expression of two components of NAD(P)H oxidase, Nox1 and Nox4.

Angiotensin II did not alter the protein expression of AMPKα; however, it increased the levels of phosphorylated AMPKα, and this increase was inhibited by either depressor agent (Fig. 4). Protein expression of matured SREBP-1 was increased by angiotensin II, and this increase was suppressed by losartan, but not by hydralazine.

We also examined the expression of several other lipid metabolism-related proteins. In the heart of control ($n=4$) and angiotensin II-

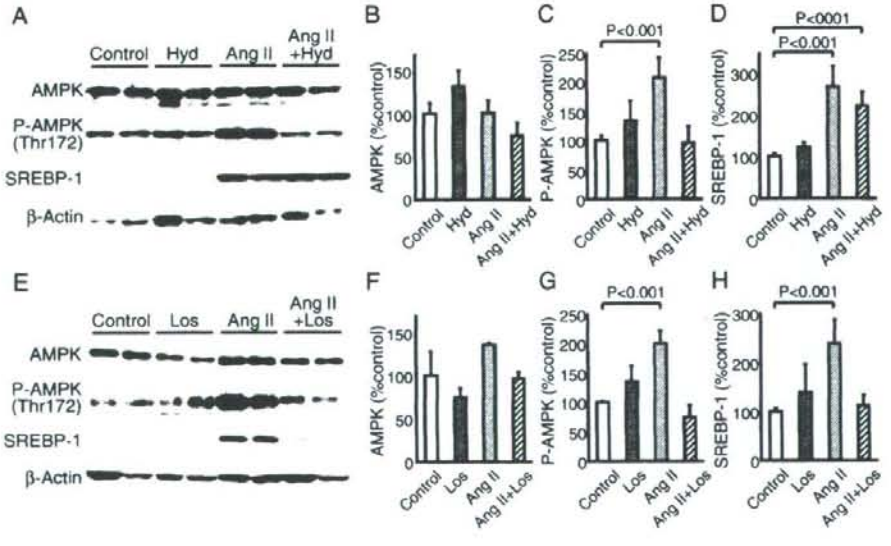

Fig. 4. Western blot analysis of AMP-activated protein kinase (AMPK), phosphorylated (activated) form of AMPKα (P-AMPK), and SREPB-1. A, E. Representative blots. B–D, F–H. Summary of data from 4–6 experiments in each group. Abbreviations are same as Table 1.